

13. COMPARISON OF LATE PLIOCENE AND LATE PLEISTOCENE SEA-SURFACE TEMPERATURES OF THE EQUATORIAL ATLANTIC DIVERGENCE¹

K. Karlin,² W. F. Ruddiman,² and A. McIntyre^{2,3}

ABSTRACT

The record of planktonic foraminifer abundances at Site 662 during the late Pliocene (~1.7–2.1 Ma) was examined to determine variations in estimated sea-surface temperature (SST). We compared the results to SST estimates from a late Pleistocene record (~1.5–200 ka) from nearby piston core RC24-7. Within the primary orbital band (~20–100 k.y.), the cold-season responses of both equatorial Atlantic records are dominated by the precessional period, and the computed range of variability is quite similar. This is in contrast to the evolution of the dominant climatic response from 41 to 100 k.y. at high northern latitudes between the late Pliocene and the late Pleistocene. The orbital-band SST response in this region of greatest divergence in the equatorial Atlantic has not changed appreciably between the late Pliocene and the late Pleistocene.

INTRODUCTION

The primary goal of this study was to assess the nature of equatorial Atlantic sea-surface temperature (see "Methods" section, this chapter) variations in the late Pliocene. Both the high-latitude North Atlantic surface ocean and Northern Hemisphere ice sheets experienced a shift in rhythm (from 41 to 100 k.y.) and an increase in amplitude of response during the middle Pleistocene (Shackleton and Opdyke, 1973; Pisias and Moore, 1981; Prell, 1982; Ruddiman et al., 1986c). We sought to determine if these changes are reflected in the sea-surface temperature (SST) signal of the late Pliocene equatorial Atlantic, in comparison with SST variations of the late Pleistocene.

To this end, the record of relative abundance changes of planktonic foraminifers from a portion of the late Pliocene (~1.7–2.1 Ma) at Site 662 of Ocean Drilling Project (ODP) Leg 108 was examined. Estimates of SST were derived from seven species determined to be the most significant contributors to the SST signal in the eastern equatorial Atlantic Ocean during the late Pleistocene (Karlin, 1986). All seven species have stratigraphic ranges extending back to at least 2.1 Ma.

Site 662 (1°23.41'S, 11°44.35'W), at a water depth of 3824 m, is located in the region most affected by seasonal equatorial divergence today, beneath the South Equatorial Current. It is situated within 21 km of piston core RC24-7 (1°20.5'S, 11°55.3'W; 3899-m water depth), which has been analyzed for foraminiferal content of approximately the last 200 k.y. (Imbrie et al., in press). The two are so close spatially (Fig. 1) that water-mass characteristics above the cores are, in effect, identical. These two records are the basis for comparison between late Pleistocene and late Pliocene signals.

Hole 662A was continuously cored down to 200 m below seafloor (mbsf), whereas intermittent segments of sediment at Hole 662B were recovered. Multiple-hole coring with the hydraulic piston corer (HPC) has provided a virtually complete sediment record across the time span reported here. Faunal analysis was initiated at the top of Section 108-

662A-14H-1 and ended at the base of Section 108-662A-15H-7. A portion of Hole 662B was spliced in for continuity.

The late Pliocene section studied is dominantly nannofossil ooze; clay and larger microfossils are minor constituents. Some interbedded layers of siliceous nannofossil ooze are also present in Core 108-662A-14H. The planktonic foraminifers exhibit good to moderate preservation.

METHODS

Samples about 10 ml in size were taken at approximately 10-cm intervals throughout Cores 108-662A-14H and 108-662A-15H and in the intervening splice of Core 108-662B-6H. This corresponds to a sampling interval of about 2.4 k.y., more than sufficient to detect orbital periodicities without signal aliasing.

For faunal analysis, samples were alternately shaken in a sodium metaphosphate solution for disaggregation, wet-sieved through a 63-μm mesh, and dried at <40°C, a total of three times. For a complete description of sample preparation, see McIntyre et al. (1989).

The dry >63-μm size fraction was then randomly split to obtain at least 275 planktonic foraminifers (half of the shell or greater) larger than 150 μm in size. The traditional counting method involves complete species identification of 300 or more individuals per level; some 29 extant species are used in SST estimation in the Atlantic Ocean F20 transfer function (Imbrie et al., in press; SPECMAP Archive 1, 1989). Ruddiman and Esmay (1986) have shown that low to moderate differences (<0.7°C) exist between SST values obtained from counts of over 300 vs. those from fewer than 250 individuals from three North Atlantic cores. We have found this to be true also in the equatorial Atlantic. The acceptable minimum number of individuals considered per sample in this study was 275.

We also analyzed the δ¹⁸O values of the planktonic foraminifer *Globigerinoides ruber* (var. white) for the entire late Pliocene interval across which faunal counts were made. The average sampling interval for δ¹⁸O analyses was also about 10 cm. The *G. ruber* specimens of the >250-μm size fraction were analyzed with a Carousel-48 automatic carbonate preparation device attached to a Finnegan-MAT-251 mass spectrometer. Calibration to the PDB standard is via the NBS-16, NBS-17, and NBS-20 standards.

QUICK-COUNT METHOD

Tests on four equatorial Atlantic piston cores (Karlin, 1986) have shown that the significant orbital periodicities found in the late Pleistocene paleotemperature signal of this region are reproduced when just seven species out of the 29 that compose the F20 equation are counted. Our method, then, depends not on a new transfer function but rather on the

¹ Ruddiman, W., Sarnthein, M., et al., 1989. Proc. ODP, Sci. Results, 108: College Station, TX (Ocean Drilling Program).

² Lamont-Doherty Geological Observatory, Palisades, NY 10964.

³ Queens College, City University of New York, Flushing, NY 11367.

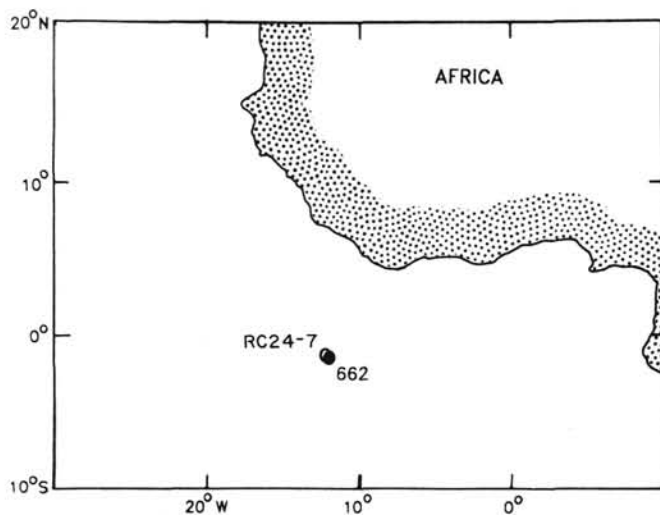


Figure 1. Locations of Site 662 ($1^{\circ}23.41'S$, $11^{\circ}44.35'W$; 3824 m) and piston core RC24-7 ($1^{\circ}20.5'S$, $11^{\circ}55.3'W$; 3899 m).

use of a subset of species from the existing F20 equation. Although calculating a new transfer function based on only the seven species would be a reasonable alternate approach, the results of our method ("SP7") speak for themselves (see Fig. 2 and Tables 1 and 2). The SP7 method maintains the relative abundances of the species considered in the same proportions as in full assemblage counts. A similar quick-counting technique was proven useful by Ruddiman and Esmay (1986), who successfully reproduced the main characteristics of the surface-water response in the high-latitude North Atlantic with just four species of planktonic foraminifers and an "all other species" category.

The seven species counted with the SP7 method are those exhibiting high and strongly variable relative abundances downcore, the species most likely to record environmental changes. The seven species are *Globigerinoides ruber* (var. white), *Globigerinoides sacculifer* (var. no sac), *Globigerina bulloides*, *Neogloboquadrina pachyderma* (var. dextral), *Neogloboquadrina dutertrei*, *N. pachyderma* (var. dextral)/*N. dutertrei*-intergrade (P/D-intergrade), and *Globorotalia inflata*. These species represent between 39% and 85% of the total foraminiferal assemblage in the four piston cores tested. In all four cores, reduced-count values are closer to full-count values for the cold season (T-cold) than for the warm season (T-warm), and offsets in SST estimates are generally in the warm direction (Karlin, 1986).

Piston core RC24-7, located near Site 662, is one of the cores used to determine the species most suitable for quick counting. This core has an average sedimentation rate of approximately 4.0 cm/k.y., based on orbital tuning of $\delta^{18}\text{O}$ data (Martinson et al., 1987), and has been sampled every 5 cm back to 200 ka at an average sampling interval of 1.3 k.y. (Imbrie et al., in press).

Mean SST values calculated from the full complement of 29 species ("full counts") in RC24-7 are 26.0°C and 19.4°C for the warm and cold seasons, respectively, whereas the SP7 version of this core yields mean values of 26.3°C and 19.5°C (Table 1). The differences between the two methods are minor (Fig. 2 and Table 2), considering the standard error of estimate of the F20 equation (1.3°C and 1.2°C for the warm and cold seasons, respectively; Molino et al., 1982). Overall correlation between the SP7 and full-count signals from RC24-7 is very good. The correlation coefficients between the two,

calculated in the depth domain, are 0.77 and 0.98 for the warm and cold seasons, respectively. They are highly coherent and in phase with each other in the precessional frequency band (Table 3).

Spectral analysis of the RC24-7 T-cold estimates reveals a single peak centered on 22.1 k.y. for both full and SP7 counts, accounting for 45% and 46% of total variance, respectively (Fig. 3). The SP7 method increases the total variance derived from full-count estimates, enhancing the signal's amplitude. However, the increase in variance at the precessional period is nearly proportional to the increase in total variance, so the relative enhancement of precessional variance is negligible.

The warm offset is more pronounced for T-warm results than for T-cold results. The warm-season equation is controlled by a larger number of taxa than that of the cold season, which is dominated by only a few species. Hence, the latter is more amenable to accurate representation by streamlined counts. Despite these minor discrepancies, the SP7 method closely reproduces late Pleistocene paleotemperature estimates (most notably T-cold) in the four piston cores tested, in terms of signal correlation and statistical similarity.

Random census counts of all species of planktonic foraminifers ("full counts") were also done throughout the Site 662 section as a control on quick-count SST estimates. One of every seven samples was counted in entirety. Both streamlined and full-count values will be presented so that the two counting methods can be compared.

Although we refer here to "SST" estimates, the annual temperature variation of the mixed layer is primarily due to seasonal divergence. Recent studies indicate a thermocline-depth habitat for several of the planktonic foraminifers with a preference for cooler waters (*N. dutertrei*, *N. pachyderma* [var. dextral], *G. bulloides*, and *G. inflata*; Fairbanks et al., 1982; C. Ravelo, pers. comm., 1987). Thus, it is not clear to what extent the SST estimates signify actual changes in temperature of the surface water vs. changes in the thickness of the mixed layer, which could allow normally deeper-dwelling species to flourish in the euphotic zone. Most likely, the cold portions of our SST signal incorporate both cooling of the surface water and shallowing of the thermocline (McIntyre et al., 1989).

SPLICES

To provide a continuous sedimentary column for paleoclimatic analysis, we have bridged the coring gap between Cores 108-662A-14H and 108-662A-15H by splicing in a portion of Core 108-662B-6H (Sample 108-662A-14H-7, 14 cm, is spliced to Sample 108-662B-6H-3, 79 cm; Sample 108-662A-15H-2, 11 cm, is spliced to Sample 108-662B-6H-4, 124 cm). The splices are based on both shipboard and shore-based direct observations of the cores and on correlation of %CaCO₃ analyses (Fig. 4), %coarse fraction, and SST estimates.

We made a second set of splices to provide an age estimate for the bottom of the Hole 662A section analyzed, which falls between the *Discoaster triradiatus* acme zone and the last occurrence (LO) of the *Globorotalia miocenica* datum (see "Biostratigraphy" section, this chapter). This set of splices extends the continuous composite record to the level of the LO of *G. miocenica*, allowing us to interpolate the age of the bottom of Section 108-662A-15H-7, the level at which our SST estimates ended. They were determined from both %CaCO₃ analyses (Fig. 4) and %coarse fraction, linking Cores 108-662A-15H and 108-662A-16H with Core 108-662B-7H (Sample 108-662A-15H-7, 41 cm, is spliced to Sample 108-662B-7H-3, 55 cm; Sample 108-662A-16H-2, 19 cm, is spliced to Sample 108-662B-7H-4, 95 cm).

The composite depth section is shown in Table 4. When we

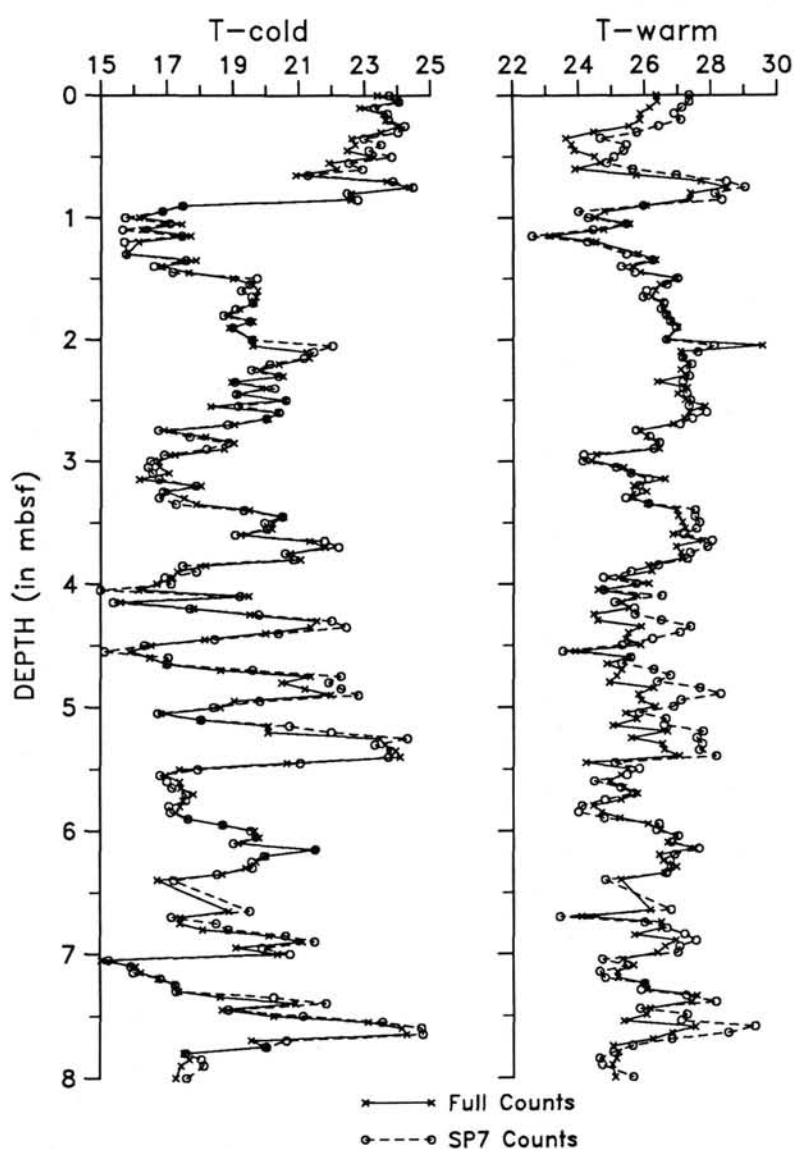


Figure 2. Estimated sea-surface temperature variations (in °C) of piston core RC24-7. Warm-season (T-warm) and cold-season (T-cold) estimates are based on full assemblage counts and quick counts with seven species (SP7).

Table 1. RC24-7 statistics of estimated sea-surface temperatures.

	Season	No. of samples	Minimum	Maximum	Mean	Variance	Standard deviation
RC24-7	T-warm	154	23.10	29.55	25.97	1.09	1.04
(full)	T-cold	154	15.03	24.36	19.36	5.24	2.29
RC24-7	T-warm	154	22.57	29.31	26.30	1.49	1.22
(SP7)	T-cold	154	14.99	24.76	19.50	6.23	2.50
RC24-7	T-warm	154	20.90	29.90	26.91	2.53	1.59
(SP6)	T-cold	154	14.27	25.45	21.25	6.50	2.55

Note: Warm-season (T-warm) and cold-season (T-cold) estimates (in °C) are based on full assemblage counts (full), quick counts with seven species (SP7), and quick counts with six species (SP6, or SP7 minus *Globorotalia inflata*).

Table 2. RC24-7 estimated sea-surface temperatures.

Depth (mbsf)	Full		SP7	
	T-warm	T-cold	T-warm	T-cold
0	26.4	23.4	27.4	23.8
0.05	26.4	24.0	27.3	24.0
0.10	26.2	22.9	27.1	23.3
0.15	25.9	23.6	26.9	23.7
0.20	25.8	23.6	27.1	23.7
0.25	25.5	24.0	26.4	24.2
0.30	24.5	23.5	25.8	24.0
0.35	23.6	22.6	24.7	23.0
0.40	23.8	22.7	25.4	23.5
0.45	23.9	22.5	25.4	23.1
0.50	24.5	23.3	25.1	23.8
0.55	24.6	21.9	24.8	22.5
0.60	23.9	22.2	25.6	22.9
0.65	25.7	20.9	27.0	21.3
0.70	27.7	23.7	28.5	23.9
0.75	28.5	24.4	29.0	24.5
0.80	27.4	22.6	28.1	22.5
0.85	27.4	22.6	28.3	22.8
0.90	26.0	17.4	26.0	17.5
0.95	24.8	16.8	24.0	16.9
1.00	24.5	16.2	24.3	15.7
1.05	25.5	17.4	25.4	17.1
1.10	24.7	16.2	24.4	15.6
1.15	23.1	17.7	22.6	17.4
1.20	24.5	16.1	24.3	15.7
1.30	25.8	15.8	25.4	15.8
1.35	26.3	17.9	26.2	17.6
1.40	25.6	16.8	25.3	16.6
1.45	25.9	17.7	25.7	17.2
1.50	26.9	19.0	27.0	19.7
1.55	26.5	19.6	26.7	19.5
1.60	26.3	19.7	26.0	19.2
1.65	26.2	19.7	25.9	19.6
1.70	26.5	19.6	26.6	19.6
1.75	26.6	19.2	26.5	19.1
1.80	26.7	18.8	26.6	18.7
1.85	26.8	19.6	26.8	19.5
1.90	27.0	18.9	26.9	19.0
2.00	26.7	19.6	26.6	19.6
2.05	29.5	19.6	28.1	22.0
2.10	27.1	21.2	27.6	21.4
2.15	27.1	21.3	27.1	21.1
2.20	27.3	20.4	27.4	20.1
2.25	27.1	19.8	27.2	19.6
2.30	27.2	20.5	27.3	20.4
2.35	26.4	18.9	27.1	19.0
2.40	27.3	20.0	27.1	20.3
2.45	27.0	19.1	27.3	19.1
2.50	27.2	20.6	27.4	20.6
2.55	27.8	18.3	27.3	19.1
2.60	27.3	20.3	27.8	20.4
2.65	27.2	20.1	27.4	20.0
2.70	26.8	19.0	27.1	18.8
2.75	25.8	16.9	25.7	16.7
2.80	26.0	18.2	26.1	17.7
2.85	26.3	19.0	26.4	18.9
2.90	26.4	18.7	26.3	18.2
2.95	24.5	17.2	24.1	16.9
3.00	24.4	16.7	24.1	16.5
3.05	25.3	16.8	25.1	16.4
3.10	25.6	17.1	25.6	16.6
3.15	26.6	16.2	26.1	16.8
3.20	25.6	18.0	25.8	17.9
3.25	26.0	16.9	25.7	16.9
3.30	25.6	17.5	25.4	16.8
3.35	26.0	17.9	26.1	17.3
3.40	27.0	19.5	27.5	19.3
3.45	27.0	20.5	27.5	20.5
3.50	27.1	20.2	27.6	20.0
3.55	27.2	20.2	27.5	20.0
3.60	26.8	19.2	27.2	19.1
3.65	27.7	21.3	28.0	21.8
3.70	26.9	21.8	27.9	22.2
3.75	27.1	20.7	27.4	20.6
3.80	27.1	21.0	27.3	20.8

Table 2 (continued).

Depth (mbsf)	Full		SP7	
	T-warm	T-cold	T-warm	T-cold
3.85	26.1	18.2	26.4	17.5
3.90	26.2	17.3	25.6	17.9
3.95	25.2	17.2	24.7	16.9
4.00	26.1	16.7	25.7	17.1
4.05	24.6	16.1	24.7	15.0
4.10	25.8	19.5	26.5	19.2
4.15	25.3	15.6	25.1	15.4
4.20	25.5	17.8	25.7	17.7
4.25	24.4	19.5	25.7	19.8
4.30	24.6	21.5	26.5	22.0
4.35	25.9	21.3	27.4	22.4
4.40	25.5	20.0	27.0	20.4
4.45	25.4	18.1	26.2	18.4
4.50	25.9	16.5	25.3	16.3
4.55	23.9	15.9	23.5	15.1
4.60	25.5	16.5	25.5	17.0
4.65	24.8	17.0	25.3	17.0
4.70	25.3	18.6	26.2	19.6
4.75	25.1	21.3	26.7	22.3
4.80	24.9	20.5	26.4	21.9
4.85	26.3	21.2	27.6	22.3
4.90	25.8	22.0	28.3	22.8
4.95	25.9	19.0	27.1	19.8
5.00	26.3	18.6	26.9	18.4
5.05	25.4	16.8	25.8	16.7
5.10	25.7	18.0	26.6	18.0
5.15	25.0	20.1	26.6	20.7
5.20	26.7	20.1	27.7	22.0
5.25	25.6	23.4	27.5	24.3
5.30	26.5	23.6	27.7	23.3
5.35	26.6	23.9	27.6	23.8
5.40	27.0	24.1	28.1	23.7
5.45	24.2	20.6	25.1	21.0
5.50	25.5	17.4	25.8	17.9
5.55	25.3	17.0	25.4	16.8
5.60	24.9	17.4	24.5	17.0
5.65	25.3	17.4	25.3	17.2
5.70	25.8	17.8	25.6	17.6
5.75	25.3	17.5	24.8	17.6
5.80	24.4	17.4	24.1	17.1
5.85	24.7	17.3	24.0	17.1
5.90	25.2	17.6	24.8	17.6
5.95	26.1	18.7	26.4	18.7
6.00	26.5	19.7	26.3	19.5
6.05	26.9	19.8	27.0	19.7
6.10	26.7	19.2	26.8	19.0
6.15	27.5	21.5	27.6	21.5
6.20	26.4	20.0	26.9	20.0
6.25	26.5	19.7	26.7	19.6
6.30	26.9	19.4	26.8	19.6
6.35	26.6	18.7	26.6	18.5
6.40	25.3	16.7	24.8	17.2
6.65	26.1	18.9	26.8	19.5
6.70	24.1	17.4	23.4	17.1
6.75	26.5	17.4	26.0	18.5
6.80	26.5	18.1	26.6	18.8
6.85	25.7	20.1	27.2	20.6
6.90	26.9	21.1	27.5	21.5
6.95	26.6	19.1	27.0	19.9
7.00	26.4	20.4	27.0	20.7
7.05	25.3	15.0	24.7	15.3
7.10	25.6	16.1	25.4	15.9
7.15	25.1	16.2	24.6	16.0
7.20	25.2	16.7	24.8	16.8
7.25	26.0	17.2	26.0	17.3
7.30	26.0	17.4	25.9	17.3
7.35	27.5	18.6	27.2	20.2
7.40	27.4	20.9	28.1	21.8
7.45	26.1	18.7	25.8	18.9
7.50	26.0	20.2	27.2	21.1
7.55	25.3	23.1	27.1	23.5
7.60	27.5	24.1	29.3	24.7
7.65	26.8	24.3	28.5	24.8
7.70	26.2	19.6	26.8	20.6
7.75	25.0	20.0	25.6	20.0

Table 2 (continued).

Depth (mbsf)	Full		SP7	
	T-warm	T-cold	T-warm	T-cold
7.80	25.2	17.5	25.0	17.6
7.85	25.1	17.7	24.6	18.0
7.90	25.0	17.4	24.7	18.1
8.00	25.1	17.3	25.6	17.6

Note: Warm-season (T-warm) and cold-season (T-cold) estimates (in °C) based on full assemblage counts (full) and quick counts with seven species (SP7).

Table 3. RC24-7 cross-spectral results of estimated sea-surface temperatures.

	Season	r	^{a,b} Coherency ²	^{a,b} Phase (k.y.)
SP7 vs. full	T-warm	0.77	0.88	-0.5
	T-cold	0.98	>0.99	0
SP6 vs. full	T-warm	0.65	0.67	-1.1
	T-cold	0.85	0.94	-0.1

Note: Warm-season (T-warm) and cold-season (T-cold) estimates (in °C) are based on full assemblage counts (full), quick counts with seven species (SP7), and quick counts with six species (SP6, or SP7 minus *Globorotalia inflata*). 95% confidence interval; bandwidth = 0.026; r = correlation coefficient.

^a At a period of 21.7 k.y.

^b Quantity listed first leads second quantity when phasing is positive.

refer to the Site 662 record, we are signifying the spliced version. We arbitrarily designated the youngest portion of our record, Sample 108-662A-14H-1, 11 cm, as 1 cm, because the slumped section above Core 108-662A-14H precludes estimation of a complete composite depth section from the sea floor to the levels used in our study.

BIOSTRATIGRAPHY

The paleomagnetic signal derived from Site 662 sediments is not sufficient to provide stratigraphic control because magnetic intensities are too weak. Shipboard age estimates for the entirety of Hole 662A are based on 14 biostratigraphic datum levels of nanofossils, planktonic foraminifera, and diatoms. An average deposition rate of 42 m/m.y. was obtained for the apparently continuous, undisturbed pelagic sediments at Site 662 between 1.4 and 3.6 Ma (Shipboard Scientific Party, 1988).

In the section we studied, there are two well-defined discoaster biostratigraphic markers (Backman, this vol.). We chose the midpoint of the range of uncertainty for each to represent these markers for time-domain analyses of Site 662. The LO of *Discoaster brouweri* (equivalent to 122.20–123.10 mbsf, or composite depths 4.90–5.80 m, Hole 662A) is considered to be a synchronous event between low and high latitudes when examined at high resolution (Backman, 1985; Baldauf et al., 1986). This event has been dated at 1.83 Ma (based on Weaver and Raymo, this vol.). The first appearance (FA) of the *D. triradiatus* acme zone (at 129.50–131.48 mbsf, or composite depths 12.18–14.16 m, Hole 662A) has been assigned an age of 2.03 Ma (based on Weaver and Raymo, this vol.). This datum is defined as the level at which *D. triradiatus* reaches 20% or more relative to *D. brouweri* (Backman and Pestiaux, 1986).

A third biostratigraphic horizon, the LO of the planktonic foraminifer *Globorotalia miocenica* at 2.18 Ma (based on Weaver and Raymo, this vol.), falls just below Section

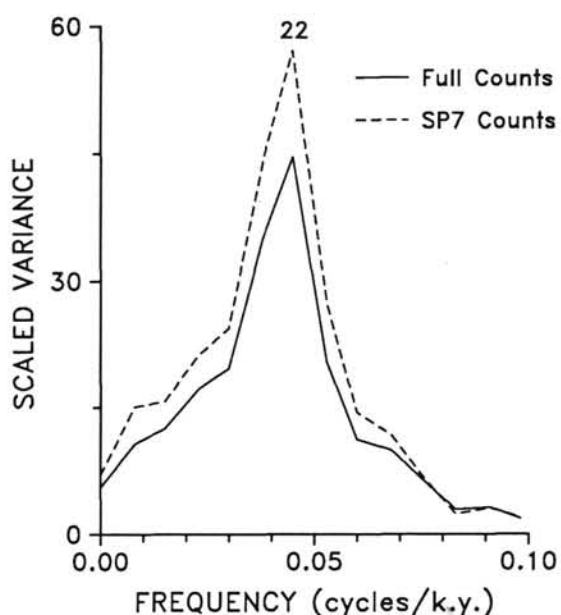


Figure 3. Variance spectra of estimated cold-season (T-cold) sea-surface temperatures of piston core RC24-7, based on full assemblage counts and quick counts with seven species (SP7). All spectra were generated by means of the Blackman-Tukey method with a lag of one-third the sample number. Labeled peaks significant at the 95% confidence interval = -0.738; bandwidth = 0.019.

108-662A-15H-7 and was used as a further time constraint. Its depth in Hole 662A has been refined subsequent to shipboard observations and assigned a range of 137.89–139.16 mbsf (composite depths 20.69–21.96 m). A core break (between Cores 108-662A-15H and 108-662A-16H) falls between this level and the oldest sample used in this study at 136.11 mbsf (composite depth of 18.79 m), but a splice with Hole 662B bridges the coring gap (see "Splices" section, this chapter).

The LO of the *G. miocenica* datum does not appear to be time-transgressive, based on other Leg 108 sites with paleomagnetic dating (Shipboard Scientific Party, 1988). It falls directly on, or quite close to, the shipboard age/depth lines. The midpoint of the range of uncertainty was chosen to represent this datum in Hole 662A (138.53 mbsf, or composite depth 21.33 m); this is close to the shipboard biostratigraphic pick of 139.00 mbsf (composite depth 21.80 m).

After revision of the three datum levels available within the section of interest, we recalculated the shipboard sedimentation rate. Linear interpolation gives sedimentation rates of 38.5 m/m.y. between the LO of *D. brouweri* and the onset of the *D. triradiatus* acme zone and 57.6 m/m.y. between the latter horizon and the LO of *G. miocenica*. The rate of 38.5 m/m.y. has been extrapolated for the sediment younger than the LO of *D. brouweri*. Cores 108-662A-14H, 108-662A-15H, and 108-662B-6H are thus dated as sediments of late Pliocene age, ranging from about 2.12 to 1.69 Ma (Fig. 5).

OXYGEN ISOTOPIC STRATIGRAPHY

In addition to dating the late Pliocene section of Site 662 biostratigraphically, we independently correlated the late Pliocene oxygen isotope record of Site 662 to that of high-latitude North Atlantic Site 607 (41°00'N, 32°58'W; Fig. 6), dated magnetostratigraphically by Raymo et al. (in press). To make this correlation, we used the graphic correlation technique of Martinson et al. (1982).

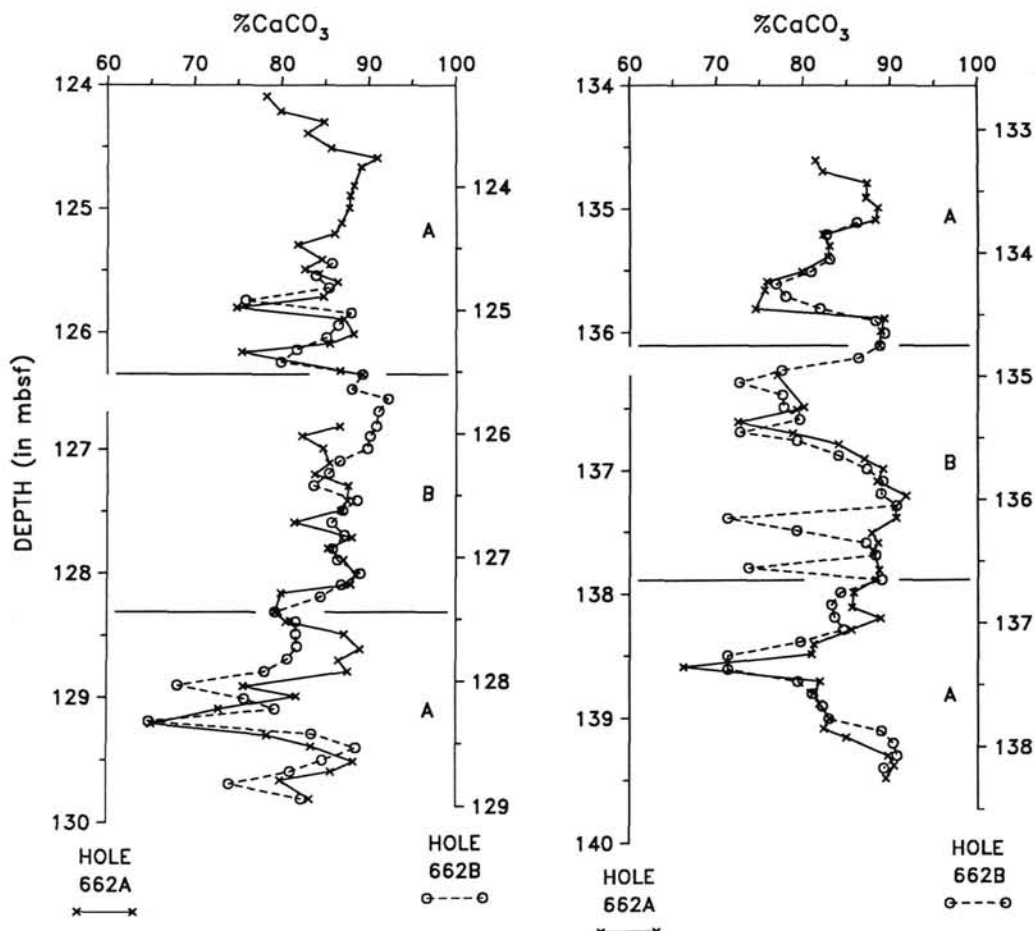


Figure 4. $\% \text{CaCO}_3$ of parts of Holes 662A and 662B, showing the splices between the two holes. For splices depicted on the left, the top splice joins Core 108-662A-14H (above the splice) to Core 108-662B-6H (below the splice); the bottom splice joins Core 108-662B-6H (above the splice) to Core 108-662A-15H (below the splice). The gap in the Hole 662A depth axis represents the coring gap of ~36 cm between Cores 108-662A-14H and 108-662A-15H. For splices depicted on the right, the top splice joins Core 108-662A-15H (above the splice) to Core 108-662B-7H (below the splice); the bottom splice joins Core 108-662B-7H (above the splice) to Core 108-662A-16H (below the splice). The gap in the Hole 662A depth axis represents the coring gap of ~7 cm between Cores 108-662A-15H and 108-662A-16H.

The results of the oxygen isotopic analyses of Site 662 for both time scales are shown in Figure 7 (Table 5). Two major trends are discernible in the data (with either time scale): (1) a long-wavelength increase in $\delta^{18}\text{O}$ values before 2 Ma and (2) moderate- to high-frequency variations throughout the record. Spectral analysis of the tuned $\delta^{18}\text{O}$ record shows that the dominant orbital periodicity is 39.8 k.y., accounting for 15.3% of the total variance; that from the biostratigraphic time scale is broader and centered at 32.0–36.0 k.y., accounting for 19.7% of the variance (Fig. 8). Thus, the $\delta^{18}\text{O}$ signal from equatorial Atlantic Site 662 oscillates at, or near, the orbital periodicity of obliquity. This is consistent with evidence that obliquity was the dominant orbital rhythm of ice-sheet response during the Matuyama (Ruddiman et al., 1986a).

There is a small amount of power in the $\delta^{18}\text{O}$ signal in the precessional frequency band. It is spread over the periods between 19.9 and 22.8 k.y. (tuned time scale) and accounts for 7.2% of the total variance (centered at 22.2 k.y., 2.9% of variance from the biostratigraphic time scale). This signifies that the ice sheets varied with minor precessional power during the late Pliocene. This, too, is consistent with high-latitude $\delta^{18}\text{O}$ evidence for late Pliocene ice sheets (Raymo et al., in press).

The largest portion of the variance in the $\delta^{18}\text{O}$ record occurs at periods at, or longer than, about 300 k.y., reflecting the long-wavelength trend visible in the $\delta^{18}\text{O}$ record. (Recall, however, that the record analyzed is only about 450 k.y. in length.) The source of this trend, which may represent long-wavelength periodic behavior or signal nonstationarity, is unknown.

The stratigraphic results of the two time scales are similar but not identical (Fig. 5). The late Pliocene section ranges between 2.12 and 1.69 Ma for the biostratigraphic time scale, and between 2.16 and 1.68 Ma for the tuned time scale. The tuned time scale overlaps the range of uncertainty in the biostratigraphic picks for the *Discoaster triradiatus* acme

Table 4. Site 662 composite depth section showing the splices between Holes 662A and 662B.

Sample 108-662A-14H-1, 11 cm
Sample 108-662A-14H-7, 14 cm → Sample 108-662B-6H-3, 79 cm
Sample 108-662A-15H-2, 11 cm ← Sample 108-662B-6H-4, 124 cm
Sample 108-662A-15H-7, 41 cm → Sample 108-662B-7H-3, 55 cm
Sample 108-662A-16H-2, 19 cm ← Sample 108-662B-7H-4, 95 cm

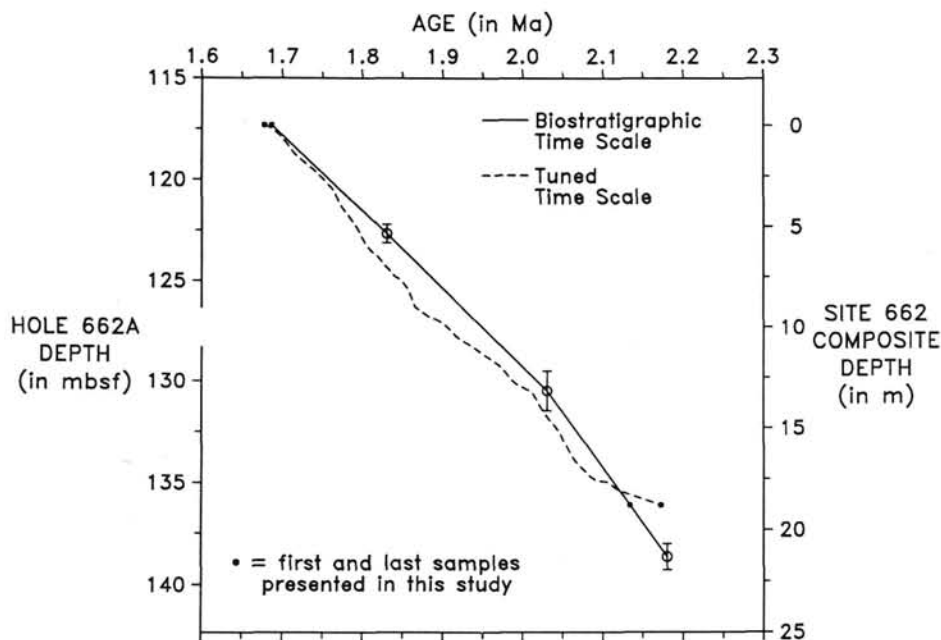


Figure 5. Age vs. depth for Hole 662A and for composite record of combined Hole 662A and Hole 662B (spliced), based on revised biostratigraphic datum levels (biostratigraphic time scale) and the results of tuning the $\delta^{18}\text{O}$ record to that of high-latitude North Atlantic Site 607 (tuned time scale). Error bars indicate uncertainty in the biostratigraphic datum levels. The gap in the Hole 662A depth axis represents the coring gap of ~36 cm between Cores 108-662A-14H and 108-662A-15H.

zone and for the extrapolated LO of *Globorotalia miocenica* but not for the LO of *Discoaster brouweri* (at which the offset ranges between 11 and 47 k.y.). We have chosen to present both time scales here because there is no definitive reason to rule one out in favor of the other.

SPECIES

Downcore variability of the seven species counted for this study is complex; each species yields a unique pattern (Fig. 9 and Table 6). All percentages signify relative abundances among the seven species, not of the total foraminiferal assemblage. The ratios among them are the same for both quick- and full-counting methods. This is the basis for the viability of the SP7 method in SST estimation. The actual percentages will, of course, be greater when only seven species are considered.

The warmest-water indicator from the euphotic zone, *Globigerinoides ruber* (var. white), is often the most abundant species observed in Site 662 sediments, with a mean of 39.5%. It is, however, quite variable, ranging between 3.9% and 74.5%. *Globigerinoides sacculifer* (var. no sac), another near-surface dweller, varies in abundance from 0.5% to 21.3%. Its statistical distribution is skewed to the low abundance side, with a mean of 6.3%.

Neogloboquadrina dutertrei, a thermocline-preferring species, is the second most common species in the overall record. Its relative abundance ranges from 5.4% to 61.9% in a nearly normal distribution. *Globorotalia inflata*, which is both a transitional water-mass indicator and a thermocline dweller, is absent at the bottom of the record, which begins just prior to this species' evolutionary FA at 2.1 Ma (Malmgren and Kennett, 1981). Although the FA of *G. inflata* was not used as a biostratigraphic marker in this study, the earliest specimens of this species in the Site 662 record are dated very close to its accepted FA. Once established in the planktonic community, the relative abundance of *G. inflata*

reaches 34.2% and is highly variable in the top third of the section.

It is difficult to quantify how the scarcity of *G. inflata* over the portion of the record prior to ~1.8 Ma affects the SST estimates. As a sensitivity test on a late Pleistocene record, we culled *G. inflata* from the SP7 species counts of piston core RC24-7 ("SP6") and then calculated SST values (Table 1). The similarity between estimates from full and SP6 counts is compelling for T-cold, giving a correlation coefficient of 0.85 (0.65 for T-warm). The SP6 estimates are highly coherent and virtually in phase with full-count values at all significant frequencies, which are shared by SP7 and SP6 results (Table 3).

We also performed this sensitivity test on the Site 662 species counts. Spectral analysis of SP6 T-cold estimates yields the same dominant orbital periodicity as that from SP7 T-cold estimates of Site 662 (see "Estimated SST" section, this chapter). Thus, although the scarcity and pre-2.1-Ma absence of *G. inflata* represents a partial no-analogue, the F20 equation is sufficiently robust that the time-varying nature of the mixed-layer response is largely reproducible even without this species.

Although the P/D-intergrade makes a significant contribution to the reliability of the SP7 method in samples of late Pleistocene age (McIntyre et al., 1989), its abundance is so low that it is of little importance in late Pliocene samples at Site 662. This "morphotype" is often absent and never reaches a relative abundance higher than 8.0%. Most of its variability occurs near the top of the record.

The relative abundance of the cool-water species *Globigerina bulloides* varies from 1.2% to 46.0% at Site 662, notably decreasing in the upper third of the section. The cold-water species *Neogloboquadrina pachyderma* (var. dextral) is, at times, surprisingly abundant at Site 662, up to 61.7%. In many samples, however, it is absent, producing a distribution that is heavily skewed toward the low side. This species is highly variable in the top portion of the record.

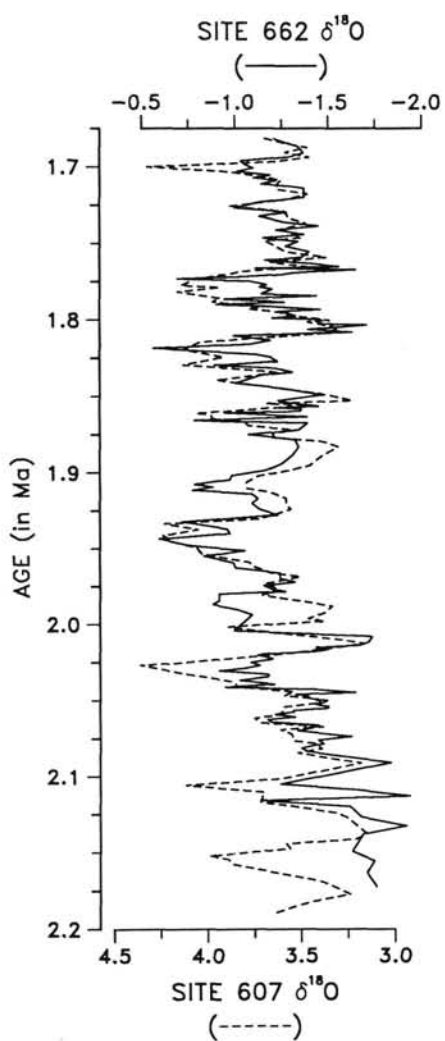


Figure 6. Variations in oxygen isotopes of the planktonic foraminifer *Globigerinoides ruber* (var. white), Site 662 (spliced), tuned to oxygen isotope variations of the benthic foraminifer *Cibicides* spp. of the high-latitude North Atlantic Site 607, both in ‰. The Site 662 record was graphically correlated to that of Site 607 to obtain the best fit.

ASSEMBLAGES

The conversion of raw census counts into assemblages, or factors, is a necessary step in the estimation of SST by factor analysis. Six factors are recognized in the F20 Atlantic Ocean equation (Molfino et al., 1982; McIntyre et al., 1989): tropical/subtropical, transitional, divergence (renamed from Kipp's [1976] gyre margin factor to fit the region of dominance better), upwelling, subpolar, and polar (Fig. 10 and Table 7).

As expected for this equatorial location, the most prominent factor extracted from the Site 662 planktonic foraminiferal record is the tropical/subtropical factor. It exhibits the highest factor loadings and the largest range of variation as well. *Globigerinoides ruber* (var. white) and, to a lesser extent, *G. sacculifer* (var. no sac) dominate this factor in the F20 transfer function.

The transitional factor exhibits a strong influence in only the top portion of the Site 662 record. The primary indicator of this factor is *Globorotalia inflata*, with a minor contribution by P/D-intergrade. Their sporadic distribution explains the

low transitional factor loadings over much of the late Pliocene section analyzed.

The divergence assemblage, which spans much of the equatorial region of the Atlantic Ocean, is fairly variable at Site 662. We counted both of the species that dominate this assemblage in the F20 equation, *Neogloboquadrina dutertrei* and *Globigerinoides sacculifer* (var. no sac). The upwelling assemblage, concentrated off the northwest and southwest coasts of Africa, is minor in value but not in range of factor loadings, and even the subpolar factor exhibits a significant amount of downcore variability at this site. The two latter factors are both represented here by *Globigerina bulloides*, *Neogloboquadrina pachyderma* (var. dextral), and the P/D-intergrade, but the species have different relative rankings of importance.

Polar faunas are virtually unrepresented in the Site 662 record. The polar factor is dominated by *N. pachyderma* (var. sinistral). This species is not a significant member of even high-latitude North Atlantic fauna until after 1.7 Ma (Raymo et al., 1986), nor is it among the seven species considered here.

Thus, the late Pliocene record at Site 662 is marked by considerable variability of five assemblages, which alternate in dominance through time. This finding is testimony to the complexity of the faunal community in this equatorial Atlantic setting.

ESTIMATED SST

The SST estimates, both full and quick counts, calculated from Site 662 samples are shown plotted vs. depth in Figure 11 (Table 8). The T-cold values (SP7 counts only) vary over a range of 10.8°C, between 14.8°C and 25.6°C. The corresponding mean value is 21.5°C. The T-warm values exhibit a range of 10.8°C, from 19.5°C to 30.3°C, with a mean of 27.4°C (Table 9), but T-warm SP7 values are less reliable than those of T-cold (see "Quick-Count Method" section, this chapter). From this point on, we will discuss the cold-season results only. Cold-season paleotemperature estimates are plotted vs. time in Figure 12.

Spectral analysis of Site 662 T-cold estimates yields different spectral signatures for the two time scales. However, the dominant periodicity in the primary orbital band (~20–100 k.y.) is precessional in both cases (Fig. 13). For the biostratigraphic time scale, it is centered on a period of 24.2 k.y. and accounts for 16.7% of the total variance. For the tuned time scale, it is centered on a period of 23.0 k.y. and accounts for 11.1% of the variance. The power spectra of Site 662 SST estimates contrast with those of the $\delta^{18}\text{O}$ record, which predominantly vary with, or near, orbital obliquity and have a minor precessional component (Fig. 8).

Most of the variance in these estimates is spread out over periods at, or longer than, about 300 k.y. This power is reflected in marked long-term changes in mean SST and variance (Fig. 12). Prior to ~2.00 Ma, the mean estimated SST is relatively low, mostly due to cold SST minima. Between ~1.85 Ma and 2.00 Ma, the SST values are characterized by a warm mean and low amplitude of variation. The portion of the record younger than ~1.85 Ma is distinguished by a cool mean SST, the result of both cold SST minima and cooler SST maxima. Because the record length of our Site 662 SST estimates is only about 450 k.y., we cannot determine if the long-term trend reflects periodic behavior or signal nonstationarity.

Could the colder SST minima in the top third of our record result solely from a gradual shift toward a faunal assemblage more like that of the Pleistocene? The top third of the record does correspond to the time in which *Globorotalia inflata*

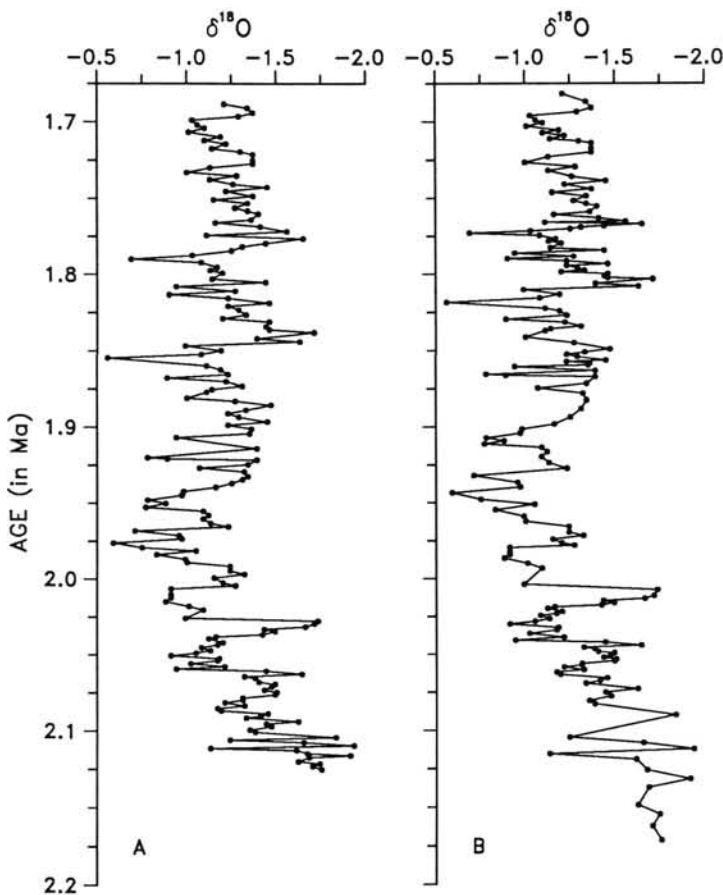


Figure 7. Variations in oxygen isotopes of the planktonic foraminifer *Globigerinoides ruber* (var. white), Site 662 (spliced). A. Biostratigraphic time scale. B. Tuned time scale.

increased in abundance at Site 662, reaching values typical of the Pleistocene. It is not coincidental that highs in the relative abundance of *G. inflata* are coeval with many of the severe lows of T-cold estimates throughout our record. However, varying *G. inflata* abundance was not the only faunal change taking place. For example, the post-1.85-Ma cold intervals are contemporaneous with an equal number of peaks in the relative abundances of both *N. pachyderma* (var. dextral) and *G. inflata*.

Although the origin of the long-term trend evident in the T-cold record is uncertain, it may be indicative of actual late Pliocene climatic changes in the divergence region of the equatorial Atlantic Ocean. This interpretation is supported, to some extent, by the existence of an equivalent long-term trend in the $\delta^{18}\text{O}$ record (Fig. 7), derived from *Globigerinoides ruber* (the trends are not in phase with one another in the two records). Thus, the evolutionary appearance of *Globorotalia inflata* is not likely to be the cause of the long-term trend in our SST record, because this event would have had no effect on the isotopic record of another species of foraminifer. The source of the long-term trends in both records remains unknown, but the trends may reflect some broad change in the climate system. Regardless, our concern is with periodic behavior within the primary orbital band.

Like the late Pliocene T-cold record from Site 662, the late Pleistocene T-cold record from piston core RC24-7 has orbital power mainly in the precessional frequency band, at 22.1 k.y. (Fig. 3). The T-cold values from core RC24-7 have a range of

9.4°C, from a low of 15.0°C to a high of 24.4°C (Fig. 2 and Tables 1 and 2). That the maxima of T-cold estimates (and, consequently, the range) are higher for quick-counted Site 662 samples than for full-counted RC24-7 samples is not surprising: the SP7 method slightly exaggerates toward the warm side (see "Quick-Count Method" section, this chapter). For example, the corresponding SP7 T-cold estimates from RC24-7 vary over a 9.8°C range, from 15.0°C to 24.8°C (Table 1).

In terms of both relative and absolute variability, therefore, the surface-water temperature signal estimated from late-Pliocene-age sediments at Site 662 closely resembles that of the late Pleistocene at core RC24-7. The cold-season SST estimates of these two cores, despite an age difference of some 2 m.y. and an evolutionary change between them, are remarkably similar in spectral character within the orbital frequency band and, to the best of our ability to estimate, in range as well.

CaCO_3

The levels of Site 662 that we analyzed for faunal content were also measured for carbonate content (Fig. 14; Ruddiman and Janecek, this vol.). With the carbonate signal, we can assess the possible impact of carbonate dissolution on our SST estimates and on interpretations of those estimates.

Some dissolution might be expected to occur at the water depth of Site 662 (3824 m). Curry and Lohmann (1986) found little evidence of dissolution in late Pleistocene piston cores from the nearby Sierra Leone Rise at a water depth of 3528 m,

Table 5. Site 662 (spliced record) oxygen isotope analyses of the planktonic foraminifer *Globigerinoides ruber* (var. white).

Core, section, interval (cm)	Composite depth (m)	$\delta^{18}\text{O}$ (‰)
108-662A-14H-1, 19	0.09	-1.21
108-662A-14H-1, 29	0.19	-1.34
108-662A-14H-1, 41	0.31	-1.37
108-662A-14H-1, 50	0.40	-1.29
108-662A-14H-1, 59	0.49	-1.03
108-662A-14H-1, 71	0.61	-1.06
108-662A-14H-1, 79	0.69	-1.10
108-662A-14H-1, 89	0.79	-1.01
108-662A-14H-1, 101	0.91	-1.19
108-662A-14H-1, 110	1.00	-1.10
108-662A-14H-1, 119	1.09	-1.22
108-662A-14H-1, 131	1.21	-1.14
108-662A-14H-1, 139	1.29	-1.30
108-662A-14H-1, 146	1.36	-1.37
108-662A-14H-2, 11	1.51	-1.37
108-662A-14H-2, 19	1.59	-1.37
108-662A-14H-2, 29	1.69	-1.13
108-662A-14H-2, 41	1.81	-1.00
108-662A-14H-2, 50	1.90	-1.28
108-662A-14H-2, 59	1.99	-1.13
108-662A-14H-2, 71	2.11	-1.26
108-662A-14H-2, 79	2.19	-1.45
108-662A-14H-2, 89	2.29	-1.22
108-662A-14H-2, 101	2.41	-1.37
108-662A-14H-2, 110	2.50	-1.15
108-662A-14H-2, 119	2.59	-1.34
108-662A-14H-2, 131	2.71	-1.27
108-662A-14H-2, 139	2.79	-1.34
108-662A-14H-2, 146	2.86	-1.40
108-662A-14H-3, 11	3.01	-1.36
108-662A-14H-3, 19	3.09	-1.16
108-662A-14H-3, 29	3.19	-1.41
108-662A-14H-3, 41	3.31	-1.56
108-662A-14H-3, 50	3.40	-1.11
108-662A-14H-3, 59	3.49	-1.65
108-662A-14H-3, 71	3.61	-1.44
108-662A-14H-3, 79	3.69	-1.31
108-662A-14H-3, 89	3.79	-1.25
108-662A-14H-3, 101	3.91	-1.03
108-662A-14H-3, 110	4.00	-0.69
108-662A-14H-3, 119	4.09	-1.08
108-662A-14H-3, 131	4.21	-1.17
108-662A-14H-3, 139	4.29	-1.13
108-662A-14H-3, 146	4.36	-1.20
108-662A-14H-4, 11	4.51	-1.14
108-662A-14H-4, 19	4.59	-1.44
108-662A-14H-4, 29	4.69	-0.94
108-662A-14H-4, 41	4.81	-1.27
108-662A-14H-4, 50	4.90	-0.90
108-662A-14H-4, 59	4.99	-1.23
108-662A-14H-4, 71	5.11	-1.46
108-662A-14H-4, 79	5.19	-1.23
108-662A-14H-4, 89	5.29	-1.29
108-662A-14H-4, 101	5.41	-1.33
108-662A-14H-4, 110	5.50	-1.20
108-662A-14H-4, 119	5.59	-1.46
108-662A-14H-4, 131	5.71	-1.44
108-662A-14H-4, 139	5.79	-1.46
108-662A-14H-4, 146	5.86	-1.71
108-662A-14H-5, 11	6.01	-1.39
108-662A-14H-5, 19	6.09	-1.63
108-662A-14H-5, 29	6.19	-0.99
108-662A-14H-5, 41	6.31	-1.19
108-662A-14H-5, 50	6.40	-1.08
108-662A-14H-5, 59	6.49	-0.56
108-662A-14H-5, 79	6.69	-1.11
108-662A-14H-5, 89	6.79	-1.19
108-662A-14H-5, 101	6.91	-1.23
108-662A-14H-5, 110	7.00	-0.89
108-662A-14H-5, 119	7.09	-1.22
108-662A-14H-5, 131	7.21	-1.31
108-662A-14H-5, 139	7.29	-1.14
108-662A-14H-5, 146	7.36	-1.11
108-662A-14H-6, 11	7.51	-1.00

Table 5 (continued).

Core, section, interval (cm)	Composite depth (m)	$\delta^{18}\text{O}$ (‰)
108-662A-14H-6, 19	7.59	-1.27
108-662A-14H-6, 29	7.69	-1.47
108-662A-14H-6, 41	7.81	-1.33
108-662A-14H-6, 50	7.90	-1.23
108-662A-14H-6, 59	7.99	-1.29
108-662A-14H-6, 71	8.11	-1.45
108-662A-14H-6, 79	8.19	-1.23
108-662A-14H-6, 89	8.29	-1.36
108-662A-14H-6, 101	8.41	-1.35
108-662A-14H-6, 110	8.50	-0.94
108-662A-14H-6, 139	8.79	-1.39
108-662A-14H-7, 11	9.01	-0.78
108-662A-14H-7, 14	9.04	-0.89
108-662B-6H-3, 82	9.07	-1.39
108-662B-6H-3, 94	9.19	-1.34
108-662B-6H-3, 102	9.27	-1.07
108-662B-6H-3, 112	9.37	-1.32
108-662B-6H-3, 124	9.49	-1.34
108-662B-6H-3, 132	9.57	-1.31
108-662B-6H-3, 142	9.67	-1.25
108-662B-6H-4, 2	9.77	-1.16
108-662B-6H-4, 12	9.87	-0.98
108-662B-6H-4, 22	9.97	-0.97
108-662B-6H-4, 34	10.09	-0.78
108-662B-6H-4, 42	10.17	-0.88
108-662B-6H-4, 52	10.27	-0.77
108-662B-6H-4, 62	10.37	-1.09
108-662B-6H-4, 73	10.48	-1.12
108-662B-6H-4, 82	10.57	-1.09
108-662B-6H-4, 93	10.68	-1.13
108-662B-6H-4, 102	10.77	-1.23
108-662B-6H-4, 112	10.87	-0.71
108-662B-6H-4, 124	10.99	-0.81
108-662A-15H-2, 11	10.99	-1.10
108-662A-15H-2, 19	11.07	-0.97
108-662A-15H-2, 29	11.17	-0.59
108-662A-15H-2, 41	11.29	-0.75
108-662A-15H-2, 50	11.38	-1.05
108-662A-15H-2, 59	11.47	-0.83
108-662A-15H-2, 71	11.59	-0.99
108-662A-15H-2, 79	11.67	-1.00
108-662A-15H-2, 89	11.77	-1.24
108-662A-15H-2, 101	11.89	-1.24
108-662A-15H-2, 110	11.98	-1.32
108-662A-15H-2, 119	12.07	-1.15
108-662A-15H-2, 131	12.19	-1.20
108-662A-15H-2, 139	12.27	-1.27
108-662A-15H-2, 146	12.34	-0.91
108-662A-15H-3, 11	12.49	-0.91
108-662A-15H-3, 19	12.57	-0.91
108-662A-15H-3, 29	12.67	-0.88
108-662A-15H-3, 41	12.79	-1.01
108-662A-15H-3, 50	12.88	-1.09
108-662A-15H-3, 71	13.09	-0.99
108-662A-15H-3, 79	13.17	-1.73
108-662A-15H-3, 89	13.27	-1.71
108-662A-15H-3, 101	13.39	-1.66
108-662A-15H-3, 110	13.48	-1.43
108-662A-15H-3, 119	13.57	-1.49
108-662A-15H-3, 131	13.69	-1.42
108-662A-15H-3, 139	13.77	-1.16
108-662A-15H-3, 146	13.84	-1.12
108-662A-15H-4, 11	13.99	-1.20
108-662A-15H-4, 19	14.07	-1.17
108-662A-15H-4, 29	14.17	-1.08
108-662A-15H-4, 41	14.29	-1.13
108-662A-15H-4, 50	14.38	-1.05
108-662A-15H-4, 59	14.47	-0.91
108-662A-15H-4, 71	14.59	-1.18
108-662A-15H-4, 79	14.67	-1.17
108-662A-15H-4, 89	14.77	-1.02
108-662A-15H-4, 101	14.89	-1.21
108-662A-15H-4, 110	14.98	-0.94
108-662A-15H-4, 119	15.07	-1.44

Table 5 (continued).

Core, section, interval (cm)	Composite depth (m)	$\delta^{18}\text{O}$ (‰)
108-662A-15H-4, 131	15.19	-1.64
108-662A-15H-4, 139	15.27	-1.32
108-662A-15H-4, 146	15.34	-1.38
108-662A-15H-5, 11	15.49	-1.40
108-662A-15H-5, 19	15.57	-1.49
108-662A-15H-5, 29	15.67	-1.47
108-662A-15H-5, 41	15.79	-1.43
108-662A-15H-5, 50	15.88	-1.50
108-662A-15H-5, 59	15.97	-1.49
108-662A-15H-5, 71	16.09	-1.31
108-662A-15H-5, 79	16.17	-1.31
108-662A-15H-5, 89	16.27	-1.21
108-662A-15H-5, 101	16.39	-1.32
108-662A-15H-5, 110	16.48	-1.17
108-662A-15H-5, 119	16.57	-1.19
108-662A-15H-5, 131	16.69	-1.45
108-662A-15H-5, 139	16.77	-1.41
108-662A-15H-5, 146	16.84	-1.33
108-662A-15H-6, 11	16.99	-1.62
108-662A-15H-6, 19	17.07	-1.44
108-662A-15H-6, 29	17.17	-1.47
108-662A-15H-6, 41	17.29	-1.35
108-662A-15H-6, 50	17.38	-1.38
108-662A-15H-6, 71	17.59	-1.83
108-662A-15H-6, 79	17.67	-1.24
108-662A-15H-6, 89	17.77	-1.65
108-662A-15H-6, 101	17.89	-1.93
108-662A-15H-6, 110	17.98	-1.13
108-662A-15H-6, 119	18.07	-1.61
108-662A-15H-6, 131	18.19	-1.67
108-662A-15H-6, 139	18.27	-1.91
108-662A-15H-6, 146	18.34	-1.68
108-662A-15H-7, 11	18.49	-1.62
108-662A-15H-7, 19	18.57	-1.74
108-662A-15H-7, 29	18.67	-1.70
108-662A-15H-7, 41	18.79	-1.75

but they found more obvious shell fragmentation and lower carbonate accumulation rates at depths greater than 3951 m. Site 662 is in the range between these depths; it is situated above the current lysocline (Takahashi et al., 1980).

If dissolution were a problem at Site 662, we would expect its effect on calculated SST values to be greatest where intervals of extremely low carbonate abundance coincide with the coldest paleotemperature estimates (Fig. 14). This is not consistently true, and cross-spectral analysis between $\% \text{CaCO}_3$ and SST estimates yields low correlation coefficients (Table 10).

Dissolution is known to remove selectively warm-water species, which tend to be fragile, thus enhancing the abundance of cold-water forms, which are usually more robust (Berger, 1968; Hutson, 1977). *Globigerinoides ruber* is one of the most fragile species of planktonic foraminifers (Ruddiman and Heezen, 1967; Parker and Berger, 1971; Thunell and Honjo, 1981). Therefore, if dissolution effects on Site 662 sediments were significant, they should be reflected in the relative abundance of this species (Fig. 14). The statistical correlation between $\% G. ruber$ (var. white) and $\% \text{CaCO}_3$ is moderate at best, arguing against dissolution control of SST (Table 10).

Low to moderate correlations between $\% \text{CaCO}_3$ and these other signals indicate that dissolution could be at most a minor contributor to the overall estimated SST signal. Nevertheless, the coherencies between $\% \text{CaCO}_3$ and both SST and $\% G. ruber$ at the precessional period are moderate to high (Table 10), which implies that dissolution could account for a substantial amount of the precessional component of the SST record.

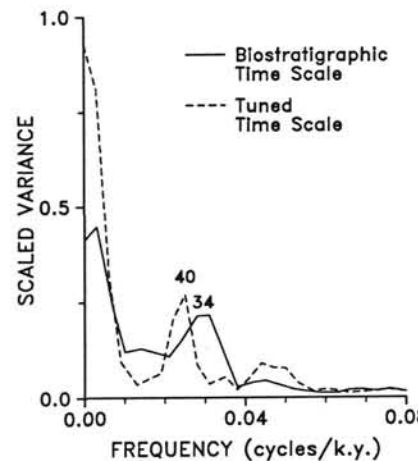


Figure 8. Variance spectra of oxygen isotopes of the planktonic foraminifer *Globigerinoides ruber* (var. white), Site 662 (spliced). Bandwidth = 0.009 and 0.008 for the biostratigraphic and tuned time scales, respectively.

Two factors argue against a strong precessional imprint of dissolution on our Site 662 SST estimates. First, the precessional components of these signals should be in phase if all are representative of dissolution effects. The phase offsets that we observe (1.4–3.4 k.y., with SST and $\% G. ruber$ leading $\% \text{CaCO}_3$ at the period of precession; Table 10) imply that the three parameters are not driven by the same forcing mechanism. Because the amount of phase offset between the carbonate record and the other signals varies substantially from cycle to cycle, this argument offers suggestive, but not definitive, evidence against dissolution control of the SST estimates.

Second, the carbonate signal is not solely a function of dissolution. The long-term mean fluxes of opal and terrigenous dust to Site 662 increased markedly during the late Pliocene, with much of the increase apparently concentrated in short-term pulses in the orbital frequency band (Fig. 14; Ruddiman and Janecek, this vol.). Periodic increases of these noncarbonate components are attributed to independent climatic responses within the equatorial-ocean mixed layer and on the African continent, thus providing an alternative explanation for the existence of carbonate minima at the precessional period.

We favor the explanation that surface climatic changes, rather than dissolution, dominate the SST, *G. ruber*, and carbonate signals. Thus, changes in surface climate would account for the moderate to high coherence between the carbonate record and the SST and $\% G. ruber$ records at the precessional period. A definitive explanation will require orbital-scale analysis of the fluxes of all components.

DISCUSSION

The primary goal of this study was to assess the nature of equatorial Atlantic SST variation in the late Pliocene. With this accomplished, our ultimate goal is to evaluate the possibility of climatic interconnections between the equatorial Atlantic Ocean and both the North Atlantic Ocean and Northern Hemisphere ice sheets.

The climatic response patterns of the late Pleistocene have been well established. The equatorial and Northern Hemisphere regions of the Atlantic have had different dominant responses over the last 300 k.y. Within the primary orbital band (~20–100 k.y.), cold-season SST records from the divergence region of the Pleistocene Atlantic Ocean predominantly oscillate at the 23-k.y. period of orbital precession,

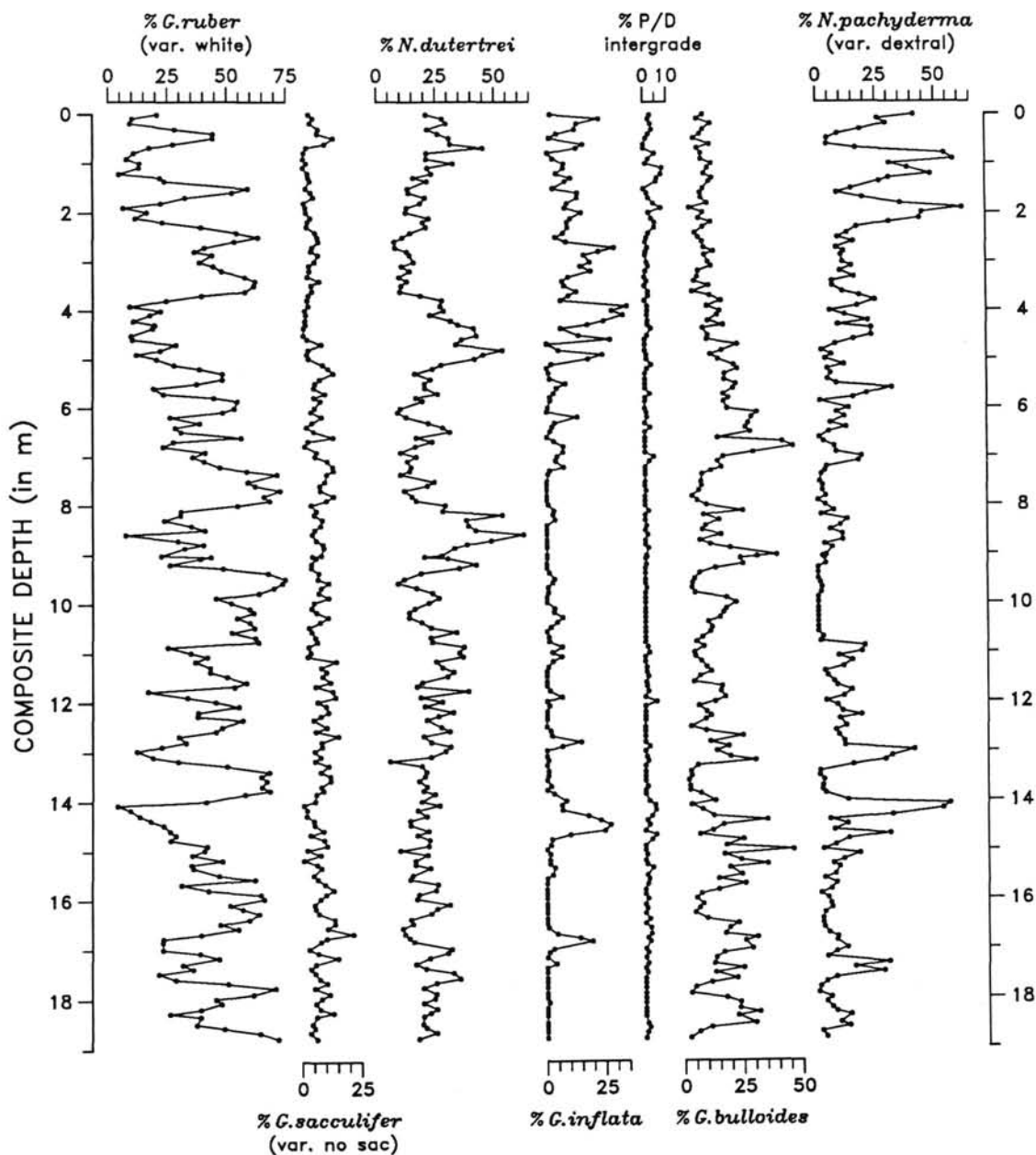


Figure 9. Variations in percent relative abundance of the seven species of planktonic foraminifers used in the SP7 method, Site 662 (spliced); %*Globigerinoides ruber* (var. white), %*G. sacculifer* (var. no sac), %*Neogloboquadrina dutertrei*, %*Globorotalia inflata*, the %P/D-intergrade, %*Globigerina bulloides*, and %*N. pachyderma* (var. dextral). Note that the percentage of each species is relative to the percentages of the other six species, not to the total species abundance.

with lesser power at the 100-k.y. period of eccentricity (McIntyre et al., 1989).

In contrast, the 100-k.y. period has dominated the SST response of the North Atlantic Ocean since the middle Pleistocene, with the obliquity (41 k.y.) and precession periods second and third in significance, respectively (Ruddiman and McIntyre, 1981, 1984). The same is true of the response of the Northern Hemisphere ice sheets, as measured by $\delta^{18}\text{O}$, used as a proxy for ice volume (Hays et al., 1976; Imbrie et al., 1984). These different dominant rhythms argue for largely independent late Pleistocene climatic responses within the orbital frequency band for the two regions under discussion.

Although the dominant orbital periods differ, these regions share some variance in the orbital frequency band. Precessional power is very strong in the SST response of the equatorial Atlantic Ocean and is also strong in that of the mid-latitude North Atlantic Ocean. The 23-k.y. period is present in the $\delta^{18}\text{O}$ response of the high-latitude ice sheets. A small amount of shared variance also exists at the period of eccentricity, although record lengths are generally too short for this to be considered statistically significant. That shared variance exists between these late Pleistocene records allows for some degree of climatic linkage of equatorial and northern regions.

Table 6. Site 662 (spliced record) percent relative abundance of the seven species of planktonic foraminifers used in the quick counts (SP7).

Core, section, interval (cm)	Composite depth (m)	Composite						
		1	2	3	4	5	6	7
108-662A-14H-1, 11	0.01	20.6	2.9	20.9	2.9	2.9	8.7	41.2
108-662A-14H-1, 11	0.01	15.6	2.2	15.9	2.2	2.2	6.6	31.1
108-662A-14H-1, 19	0.09	10.1	4.7	27.9	22.8	2.2	6.2	26.1
108-662A-14H-1, 29	0.19	9.2	3.5	29.5	13.4	3.1	11.9	29.5
108-662A-14H-1, 41	0.31	28.1	6.9	21.5	12.4	3.7	8.8	18.6
108-662A-14H-1, 50	0.40	44.2	6.5	26.0	4.8	2.2	7.4	9.1
108-662A-14H-1, 59	0.49	44.1	13.3	30.8	1.5	1.0	4.6	4.6
108-662A-14H-1, 71	0.61	27.4	9.6	31.2	15.9	0.0	11.5	4.5
108-662A-14H-1, 79	0.69	17.3	1.9	45.1	13.0	0.0	6.2	16.7
108-662A-14H-1, 89	0.79	10.8	0.8	21.1	0.8	4.6	7.7	54.2
108-662A-14H-1, 101	0.91	7.7	0.5	21.0	3.1	2.0	7.7	58.0
108-662A-14H-1, 110	1.00	13.3	2.0	32.5	7.9	1.0	12.3	31.0
108-662A-14H-1, 110	1.00	7.5	1.1	18.3	4.4	0.6	6.9	17.5
108-662A-14H-1, 119	1.09	13.1	0.5	21.6	7.5	8.0	10.6	38.7
108-662A-14H-1, 131	1.21	4.6	2.5	23.2	4.6	7.6	9.1	48.5
108-662A-14H-1, 139	1.29	21.9	2.7	15.6	10.7	5.8	12.5	30.8
108-662A-14H-1, 146	1.36	23.8	3.4	21.4	8.3	5.3	11.2	26.7
108-662A-14H-2, 11	1.51	58.9	1.5	13.2	3.1	0.0	8.5	14.7
108-662A-14H-2, 19	1.59	52.2	3.7	13.5	13.5	1.2	7.4	8.6
108-662A-14H-2, 29	1.69	32.4	4.8	20.5	13.3	1.9	7.6	19.5
108-662A-14H-2, 29	1.69	21.7	3.2	13.7	8.9	1.3	5.1	13.1
108-662A-14H-2, 41	1.81	22.0	0.8	18.4	9.0	4.1	10.2	35.5
108-662A-14H-2, 50	1.90	6.3	1.4	12.6	8.1	7.2	2.7	61.7
108-662A-14H-2, 59	1.99	16.2	1.6	12.3	15.0	2.0	8.3	44.7
108-662A-14H-2, 71	2.11	11.2	3.5	22.0	10.3	3.0	6.5	43.5
108-662A-14H-2, 79	2.19	22.8	2.2	19.4	8.9	4.4	11.7	30.6
108-662A-14H-2, 89	2.29	38.9	1.9	20.7	9.1	4.3	8.2	16.8
108-662A-14H-2, 101	2.41	53.9	5.4	13.9	7.3	1.8	4.8	12.7
108-662A-14H-2, 110	2.50	63.1	6.3	10.7	3.9	1.0	6.3	8.7
108-662A-14H-2, 119	2.59	53.2	6.9	7.4	8.5	0.5	8.0	15.4
108-662A-14H-2, 131	2.71	40.6	4.3	7.7	29.0	1.5	8.7	8.2
108-662A-14H-2, 131	2.71	25.3	2.7	4.8	18.1	0.9	5.4	5.1
108-662A-14H-2, 139	2.79	36.3	3.8	12.7	22.3	0.6	1.7	11.5
108-662A-14H-2, 146	2.86	43.8	6.7	13.8	16.1	0.4	8.9	10.3
108-662A-14H-2, 146	2.86	30.0	4.6	9.5	11.0	0.3	6.4	7.0
108-662A-14H-3, 11	3.01	38.3	5.2	15.5	18.6	1.0	10.4	10.9
108-662A-14H-3, 19	3.09	44.2	2.9	10.4	14.6	1.7	11.7	14.6
108-662A-14H-3, 29	3.19	47.7	3.1	13.9	19.0	0.5	6.2	9.7
108-662A-14H-3, 41	3.31	57.6	2.2	9.4	9.4	0.0	5.8	15.6
108-662A-14H-3, 50	3.40	61.9	7.2	12.6	6.7	0.9	4.5	6.3
108-662A-14H-3, 59	3.49	61.4	3.8	10.2	7.6	0.0	10.6	6.4
108-662A-14H-3, 71	3.61	57.7	4.1	9.7	12.8	1.5	3.6	10.7
108-662A-14H-3, 79	3.69	39.3	2.6	18.3	9.4	1.6	11.0	17.8
108-662A-14H-3, 89	3.79	24.4	2.0	27.4	6.1	0.0	15.7	24.4
108-662A-14H-3, 89	3.79	18.1	1.5	20.4	4.5	0.0	11.7	18.1
108-662A-14H-3, 101	3.91	9.0	2.5	26.6	34.2	1.1	9.7	16.9
108-662A-14H-3, 110	4.00	21.9	1.0	28.1	27.6	1.0	15.1	5.2
108-662A-14H-3, 119	4.09	17.4	1.5	22.2	32.4	1.0	14.0	11.6
108-662A-14H-3, 131	4.21	10.5	1.2	31.2	24.3	1.2	10.1	21.5
108-662A-14H-3, 139	4.29	19.7	1.5	34.3	17.5	1.5	16.8	8.8
108-662A-14H-3, 139	4.29	10.0	0.7	17.4	8.9	0.7	8.5	4.4
108-662A-14H-3, 146	4.36	18.8	0.7	40.9	6.0	2.7	8.1	22.8
108-662A-14H-4, 11	4.51	9.6	0.5	42.1	13.7	1.0	10.1	22.8
108-662A-14H-4, 19	4.59	10.2	2.0	35.7	27.0	0.0	9.7	15.3
108-662A-14H-4, 29	4.69	28.5	8.1	33.3	0.0	0.0	22.6	7.5
108-662A-14H-4, 41	4.81	21.9	2.5	52.9	5.0	0.0	16.0	1.7
108-662A-14H-4, 50	4.90	11.8	2.0	44.7	23.7	0.7	11.2	5.9
108-662A-14H-4, 59	4.99	20.3	2.6	41.2	17.6	0.6	14.4	3.3
108-662A-14H-4, 71	5.11	27.6	8.6	27.0	2.0	2.6	21.0	11.2
108-662A-14H-4, 79	5.19	38.3	10.8	23.3	0.0	0.8	22.5	4.2
108-662A-14H-4, 89	5.29	48.0	13.0	15.8	0.7	0.0	17.1	5.5
108-662A-14H-4, 101	5.41	47.9	7.3	22.4	1.2	0.0	17.0	4.2
108-662A-14H-4, 101	5.41	25.6	3.9	12.0	0.6	0.0	9.1	2.3
108-662A-14H-4, 110	5.50	37.1	5.3	19.9	7.9	0.0	21.9	7.9
108-662A-14H-4, 119	5.59	18.9	4.7	20.1	4.1	0.0	20.7	31.4
108-662A-14H-4, 131	5.71	23.1	9.4	25.5	2.8	1.9	16.5	20.8
108-662A-14H-4, 139	5.79	44.3	4.8	16.2	1.2	0.0	18.6	15.0
108-662A-14H-4, 146	5.86	54.3	7.6	19.0	1.4	0.0	16.7	0.9
108-662A-14H-4, 146	5.86	31.4	4.4	11.0	0.8	0.0	9.6	0.6
108-662A-14H-5, 11	6.01	53.0	5.2	9.9	0.5	0.0	18.3	13.1
108-662A-14H-5, 19	6.09	48.2	3.7	8.6	0.0	0.6	30.9	8.0
108-662A-14H-5, 29	6.19	26.0	8.1	12.2	13.0	0.8	28.5	11.4
108-662A-14H-5, 41	6.31	38.5	4.1	21.6	3.4	0.0	27.0	5.4
108-662A-14H-5, 50	6.40	28.1	1.8	27.7	2.2	2.2	25.9	12.1
108-662A-14H-5, 59	6.49	30.6	4.8	30.6	1.4	0.0	27.9	4.8

Table 6 (continued).

Core, section, interval (cm)	Composite depth (m)	Composite						
		1	2	3	4	5	6	7
108-662A-14H-5, 59	6.49	11.8	1.8	11.8	0.5	0.0	10.7	1.8
108-662A-14H-5, 71	6.61	55.9	13.0	16.4	0.0	0.0	14.1	0.6
108-662A-14H-5, 79	6.69	27.4	2.4	23.2	3.0	0.0	41.5	2.4
108-662A-14H-5, 89	6.79	23.0	1.0	16.0	7.0	0.0	46.0	7.0
108-662A-14H-5, 101	6.91	40.8	5.8	9.7	6.8	0.0	29.1	7.8
108-662A-14H-5, 110	7.00	35.5	5.3	16.4	4.2	3.7	16.4	18.5
108-662A-14H-5, 119	7.09	40.3	10.4	12.7	3.6	1.8	14.0	17.2
108-662A-14H-5, 131	7.21	46.8	12.8	14.2	7.1	0.0	15.6	3.5
108-662A-14H-5, 139	7.29	58.2	12.9	13.5	1.2	0.0	11.2	2.9
108-662A-14H-5, 146	7.36	71.0	10.1	9.7	0.5	0.0	7.4	1.4
108-662A-14H-6, 11	7.51	58.9	9.5	24.0	0.0	0.0	7.0	0.6
108-662A-14H-6, 19	7.59	61.9	7.4	21.2	0.0	0.0	7.4	2.1
108-662A-14H-6, 19	7.59	34.7	4.2	11.9	0.0	0.0	4.2	1.2
108-662A-14H-6, 29	7.69	72.4	7.6	11.4	0.0	0.5	6.2	1.9
108-662A-14H-6, 41	7.81	65.6	13.3	14.6	0.0	0.0	3.3	3.3
108-662A-14H-6, 50	7.90	68.0	10.2	16.4	0.0	0.0	5.5	0.0
108-662A-14H-6, 59	7.99	54.4	3.8	28.8	0.6	0.0	9.4	3.1
108-662A-14H-6, 71	8.11	30.6	6.0	27.6	3.0	1.5	24.6	6.7
108-662A-14H-6, 71	8.11	14.4	2.8	13.0	1.4	0.7	11.6	3.2
108-662A-14H-6, 79	8.19	30.4	5.0	52.8	2.5	0.0	8.1	1.2
108-662A-14H-6, 89	8.29	23.6	8.4	37.6	3.4	0.0	14.6	12.4
108-662A-14H-6, 101	8.41	34.9	7.7	38.5	0.0	0.6	8.9	9.5
108-662A-14H-6, 101	8.41	20.1	4.4	22.1	0.0	0.3	5.1	5.4
108-662A-14H-6, 110	8.50	40.7	5.1	41.6	0.0	0.0	7.5	5.1
108-662A-14H-6, 119	8.59	7.2	4.1	61.9	0.0	1.0	15.5	10.3
108-662A-14H-6, 131	8.71	29.2	5.8	48.0	0.0	0.0	6.5	10.4
108-662A-14H-6, 139	8.79	40.0	8.6	37.8	0.0	0.0	10.8	2.7
108-662A-14H-6, 146	8.86	32.0	9.0	32.5	0.0	1.3	19.2	6.0
108-662A-14H-7, 11	9.01	22.2	7.9	27.1	0.0	0.5	38.9	3.5
108-662A-14H-7, 14	9.04	43.1	4.2	19.8	0.0	0.6	30.5	1.8
108-662B-6H-3, 82	9.07	38.8	5.6	29.6	0.0	0.0	23.5	2.5
108-662B-6H-3, 82	9.07	21.2	3.1	16.2	0.0	0.0	12.8	1.4
108-662B-6H-3, 94	9.19	26.0	4.0	41.8	0.0	0.4	24.7	3.1
108-662B-6H-3, 102	9.27	48.3	3.8	34.6	0.0	0.0	13.2	0.0
108-662B-6H-3, 112	9.37	67.4	6.9	18.4	0.9	0.0	6.4	0.0
108-662B-6H-3, 124	9.49	74.5	6.6	11.3	3.3	0.0	4.3	0.0
108-662B-6H-3, 132	9.57	73.5	11.1	8.6	2.5	0.0	3.4	0.9
108-662B-6H-3, 142	9.67	69.7	8.0	16.5	0.5	0.5	3.2	1.6
108-662B-6H-4, 2	9.77	63.5	6.9	23.3	0.6	0.0	4.4	1.3
108-662B-6H-4, 12	9.87	45.3	11.1	26.0	0.0	0.0	17.7	0.0
108-662B-6H-4, 22	9.97	51.8	4.9	21.7	0.0	0.0	21.7	0.0
108-662B-6H-4, 34	10.09	59.5	3.9	15.7	3.3	0.0	17.6	0.0
108-662B-6H-4, 34	10.09	21.7	1.4	5.7	1.2	0.0	6.4	0.0
108-662B-6H-4, 42	10.17	61.2	6.0	13.4	3.0	0.0	16.4	0.0
108-662B-6H-4, 52	10.27	54.2	10.8	13.3	6.7	0.0	15.0	0.0
108-662B-6H-4, 62	10.37	59.6	7.4	18.6	4.3	0.0	9.9	0.0
108-662B-6H-4, 73	10.48	61.5	2.8	22.5	1.6	0.0	11.5	0.0
108-662B-6H-4, 82	10.57	51.9	3.9	33.3	0.0	0.0	10.9	0.0
108-662B-6H-4, 93	10.68	61.9	5.4	22.5	0.7	0.0	7.5	2.0
108-662B-6H-4, 102	10.77	63.4	6.4	23.3	1.0	0.0	4.9	1.0
108-662B-6H-4, 102	10.77	31.7	3.2	11.6	0.5	0.0	2.5	0.5
108-662B-6H-4, 112	10.87	25.1	2.7	36.6	6.6	1.1	8.2	19.7
108-662B-6H-4, 124	10.99	28.8	1.8	44.8	3.1	0.6	7.4	13.5
108-662A-15H-2, 11	10.99	40.7	5.4	24.5	1.8	3.0	1.2	23.4
108-662A-15H-2, 19	11.07	41.7	2.4	36.2	6.3	0.0	4.7	8.7
108-662A-15H-2, 29	11.17	36.6	14.4	24.8	2.6	0.0	7.2	14.4
108-662A-15H-2, 41	11.29	43.0	8.1	27.5	0.7	0.7	9.4	10.7
108-662A-15H-2, 50	11.38	42.9	10.2	32.2	0.0	0.6	11.3	2.8
108-662A-15H-2, 59	11.47	50.0	8.6	29.6	0.0	1.3	6.6	4.0
108-662A-15H-2, 71	11.59	58.2	11.9	18.9	0.0	0.4	4.0	6.6
108-662A-15H-2, 79	11.67	53.2	5.6	16.7	0.0	0.8	15.9	7.9
108-662A-15H-2, 89	11.77	16.7	12.8	38.5	1.3	1.3	15.4	14.1
108-662A-15H-2, 101	11.89	33.3	14.0	18.3	6.4	0.0	17.2	10.8
108-662A-15H-2, 101	11.89	8.7	3.7	4.8	1.7	0.0	4.5	2.8
108-662A-15H-2, 110	11.98	45.2	6.4	27.4	0.0	4.8	12.9	3.2
108-662A-15H-2, 119	12.07	55.0	10.0	20.0	1.0	0.0	6.0	8.0
108-662A-15H-2, 131	12.19	37.8	10.9	31.9	0.0	0.0	9.2	10.1
108-662A-15H-2, 139	12.27	37.5	7.6	25.7	0.0	0.0	11.1	18.1
108-662A-15H-2, 146	12.34	56.5	4.8	20.8	0.0	0.0	8.9	8.9
108-662A-15H-3, 11	12.49	47.9	10.4	27.1	0.0	0.0	2.8	11.8
108-662A-15H-3, 19	12.57	45.5	5.8	30.6	1.6	0.0	9.1	7.4
108-662A-15H-3, 19	12.57	19.2	2.4	12.9	0.7	0.0	3.8	3.1
108-662A-15H-3, 29	12.67	29.7	15.2	19.6	2.2	0.0	24.6	8.7
108-662A-15H-3, 41	12.79	32.7	8.2	22.7	14.6	0.0	10.9	10.9
108-662A-15H-3, 41	12.79	12.1	3.0	8.4	5.4	0.0	4.0	4.0
108-662A-15H-3, 50	12.88	22.4	8.4	30.8	6.5	1.9	18.7	11.2

Table 6 (continued).

Core, section, interval (cm)	Composite depth (m)							
		1	2	3	4	5	6	7
108-662A-15H-3, 59	12.97	12.0	5.2	28.8	0.0	0.0	13.6	40.3
108-662A-15H-3, 71	13.09	18.7	7.7	22.6	0.0	0.6	19.4	31.0
108-662A-15H-3, 79	13.17	29.3	5.4	5.4	0.6	1.2	29.9	28.1
108-662A-15H-3, 89	13.27	50.0	11.1	18.8	0.0	0.0	5.6	14.6
108-662A-15H-3, 101	13.39	67.7	7.7	20.6	0.6	0.0	2.6	0.6
108-662A-15H-3, 110	13.48	64.4	11.7	20.0	0.5	0.0	2.9	0.5
108-662A-15H-3, 119	13.57	66.7	11.9	17.5	0.0	0.0	1.7	2.3
108-662A-15H-3, 119	13.57	34.4	6.1	9.0	0.0	0.0	0.9	1.2
108-662A-15H-3, 131	13.69	64.6	8.0	20.8	1.8	0.9	2.2	1.8
108-662A-15H-3, 139	13.77	68.0	8.8	19.3	0.0	0.0	2.2	1.7
108-662A-15H-3, 146	13.84	57.5	5.8	24.1	2.9	0.0	6.8	2.9
108-662A-15H-4, 11	13.99	41.2	5.3	18.7	8.0	1.6	12.8	12.3
108-662A-15H-4, 19	14.07	3.9	0.7	26.3	6.4	4.3	2.8	55.5
108-662A-15H-4, 29	14.17	9.4	2.1	17.1	6.6	4.5	7.7	52.6
108-662A-15H-4, 41	14.29	13.3	1.9	20.9	17.5	2.8	12.3	31.3
108-662A-15H-4, 41	14.29	9.2	1.3	14.5	12.2	2.0	8.6	21.8
108-662A-15H-4, 50	14.38	17.9	4.9	13.8	22.8	0.8	35.0	4.9
108-662A-15H-4, 59	14.47	23.4	5.3	14.0	26.9	1.8	16.4	12.3
108-662A-15H-4, 71	14.59	26.1	9.0	21.6	24.6	0.0	11.9	6.7
108-662A-15H-4, 79	14.67	28.5	3.5	16.9	9.9	4.7	6.4	30.2
108-662A-15H-4, 89	14.77	26.2	9.2	22.0	2.1	2.8	24.8	12.8
108-662A-15H-4, 101	14.89	41.6	10.4	21.6	1.6	0.0	17.6	7.2
108-662A-15H-4, 101	14.89	16.3	4.1	8.5	0.6	0.0	6.9	2.8
108-662A-15H-4, 110	14.98	40.4	2.0	9.6	0.0	0.0	46.0	2.0
108-662A-15H-4, 119	15.07	35.3	7.7	21.1	1.3	0.6	16.7	17.3
108-662A-15H-4, 131	15.19	47.9	0.6	16.0	1.2	0.0	23.7	10.6
108-662A-15H-4, 139	15.27	35.0	6.1	15.9	1.2	0.6	35.0	6.1
108-662A-15H-4, 146	15.34	35.7	7.9	22.2	3.2	3.2	19.0	8.7
108-662A-15H-5, 11	15.49	46.5	4.7	14.7	2.3	0.8	24.0	7.0
108-662A-15H-5, 19	15.57	61.8	6.4	13.7	0.0	1.5	14.2	2.5
108-662A-15H-5, 29	15.67	30.9	9.6	25.5	0.0	1.1	25.5	7.4
108-662A-15H-5, 29	15.67	15.5	4.8	12.8	0.0	0.5	12.8	3.7
108-662A-15H-5, 41	15.79	42.2	13.3	24.7	0.0	0.0	14.5	5.4
108-662A-15H-5, 50	15.88	64.3	10.1	17.6	0.0	0.0	7.0	1.0
108-662A-15H-5, 59	15.97	65.7	7.6	16.7	0.0	1.0	5.1	4.0
108-662A-15H-5, 71	16.09	51.3	5.2	30.5	0.0	0.0	7.8	5.2
108-662A-15H-5, 79	16.17	56.6	5.6	25.2	0.0	0.7	6.3	5.6
108-662A-15H-5, 89	16.27	63.5	7.0	22.6	0.0	0.0	4.3	2.6
108-662A-15H-5, 89	16.27	25.0	2.7	8.9	0.0	0.0	1.7	1.0
108-662A-15H-5, 101	16.39	59.4	13.5	14.1	0.0	1.8	9.4	1.8
108-662A-15H-5, 110	16.48	47.0	13.7	14.9	0.0	0.0	22.6	1.8
108-662A-15H-5, 119	16.57	54.8	10.6	10.6	0.6	2.2	19.0	2.2
108-662A-15H-5, 131	16.69	39.0	21.3	11.6	4.3	2.4	17.1	4.3
108-662A-15H-5, 139	16.77	23.1	10.2	13.4	13.9	0.9	30.6	7.9
108-662A-15H-5, 146	16.84	22.9	7.6	15.3	19.1	1.9	25.5	7.6
108-662A-15H-6, 11	16.99	22.9	2.8	31.2	2.8	0.0	28.4	11.9
108-662A-15H-6, 11	16.99	7.7	0.9	10.5	0.9	0.0	9.5	4.0
108-662A-15H-6, 19	17.07	38.5	6.6	29.5	0.8	0.8	16.4	7.4
108-662A-15H-6, 29	17.17	46.5	14.9	21.9	0.0	0.0	13.2	3.5
108-662A-15H-6, 41	17.29	31.4	5.7	16.2	3.8	0.9	12.4	29.5
108-662A-15H-6, 50	17.38	35.8	3.7	20.4	0.0	0.0	24.8	15.3
108-662A-15H-6, 59	17.47	21.4	5.3	32.1	0.0	0.8	13.0	27.5
108-662A-15H-6, 71	17.59	28.4	7.3	34.9	0.0	0.0	22.0	7.3
108-662A-15H-6, 79	17.67	50.4	10.4	24.8	0.0	0.0	11.2	3.2
108-662A-15H-6, 89	17.77	70.3	5.2	19.4	0.0	0.0	4.5	0.6
108-662A-15H-6, 101	17.89	61.1	11.5	24.8	0.0	0.0	2.7	0.0
108-662A-15H-6, 110	17.98	45.3	8.0	24.1	0.0	0.0	17.5	5.1
108-662A-15H-6, 119	18.07	47.6	5.7	19.4	0.8	0.0	23.4	3.2
108-662A-15H-6, 131	18.19	38.9	7.4	25.0	0.0	0.0	23.1	5.6
108-662A-15H-6, 131	18.19	11.2	2.1	7.2	0.0	0.0	6.7	1.6
108-662A-15H-6, 139	18.27	25.9	13.0	22.2	0.0	0.0	31.5	7.4
108-662A-15H-6, 146	18.34	38.8	6.0	19.4	0.0	0.0	22.4	13.4
108-662A-15H-7, 11	18.49	37.2	4.1	19.0	0.0	0.8	29.8	9.1
108-662A-15H-7, 19	18.57	48.7	5.1	20.5	0.0	1.7	11.1	12.8
108-662A-15H-7, 29	18.67	63.8	3.4	24.8	0.0	0.7	6.0	1.3
108-662A-15H-7, 41	18.79	71.4	6.0	17.3	0.0	0.0	2.3	3.0

Note: 1 = *Globigerinoides ruber* (var. white); 2 = *G. sacculifer* (var. no sac); 3 = *Neogloboquadrina dutertrei*; 4 = *Globorotalia inflata*; 5 = P/D-intergrade; 6 = *Globigerina bulloides*; and 7 = *N. pachyderma* (var. dextral). Full assemblage counts (second value listed) and quick counts with seven species (first value listed) are given; spliced record.

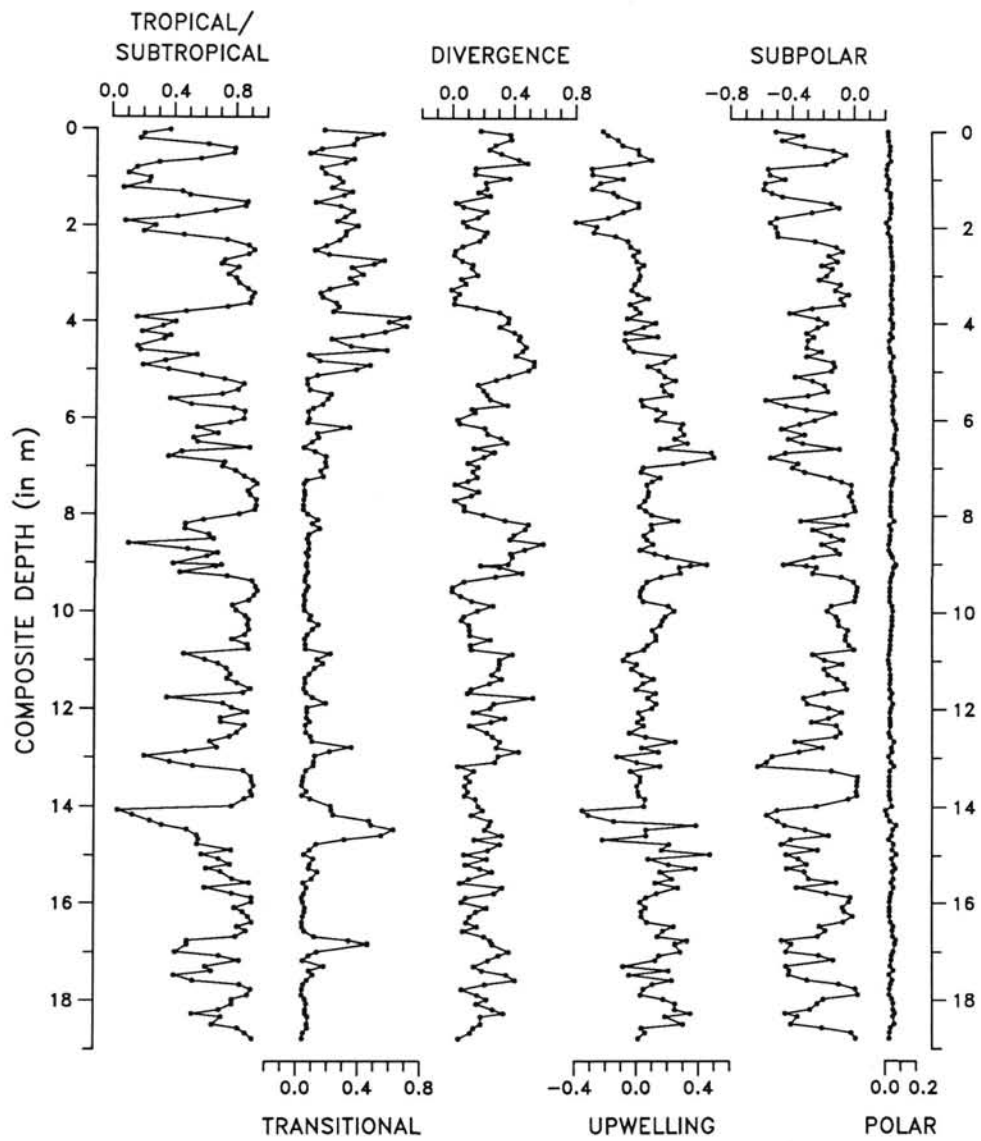


Figure 10. Variations in factor loadings of the six assemblages derived from the F20 Atlantic Ocean transfer function (tropical/subtropical, transitional, divergence, upwelling, subpolar, and polar), based on quick counts with seven species, Site 662 (spliced). Factor loadings can vary between +1.0 and -1.0.

The precessional components of the late Pleistocene climatic responses in the two regions are, however, not in phase. The precessional component of equatorial Atlantic SST leads that of high-latitude ice volume by ~2.7 k.y. and that of North Atlantic SST by ~6.3 k.y. (McIntyre et al., 1989). Even this lead, however, does not rule out the possibility of climatic interconnections between the equatorial and Northern Hemisphere regions; we suggest that the phasing of a response in one region may reflect the combined influences of several regions with different phasing.

Recent evidence (Ruddiman et al., 1986c) points to 41 k.y. as the dominant orbital rhythm of the Northern Hemisphere ice-volume and North Atlantic SST responses during most of the early Pleistocene and late Pliocene, and as far back as the onset of extensive Northern Hemisphere glaciation at 2.45 Ma (Backman, 1979; Shackleton et al., 1984; Zimmerman et al., 1985; Ruddiman et al., 1986b). In these Northern Hemisphere records, power at the frequencies of eccentricity and preces-

sion is present but weak (Raymo et al., in press). Also, the amplitude of $\delta^{18}\text{O}$ and SST variations during the Matuyama reversed magnetic chron was only half that of the Brunhes normal chron in the high-latitude North Atlantic (Shackleton et al., 1984; Ruddiman et al., 1986d).

In contrast, the planktonic foraminiferal evidence we have presented shows that this region of the equatorial Atlantic responded in the cold season in much the same manner during the late Pliocene as it did during the late Pleistocene. The T-cold estimates from Site 662 samples, dated as ~1.7 to 2.1 Ma, vary by an amplitude of about 9°C (T-cold), as do samples from nearby piston core RC24-7, ranging in age from ~0 to 200 ka. Also, the dominant orbital frequency at which SST estimates from both time intervals oscillate is that of precession. These relatively unchanging responses are in sharp contrast to those of the North Atlantic Ocean and Northern Hemisphere ice sheets, which increased considerably in amplitude and changed in dominant rhythm between the late

Table 7. Site 662 (spliced record) factor loadings based on the F20 Atlantic Ocean transfer function.

Core, section, interval (cm)	Composite depth (m)	Tropical/subtropical	Transitional	Divergence	Upwelling	Subpolar	Polar
108-662A-14H-1, 11	0.01	0.3707	0.1660	0.1783	-0.2270	-0.5095	0.0158
108-662A-14H-1, 11	0.01	0.3973	0.1688	0.2044	-0.2224	-0.5464	0.0190
108-662A-14H-1, 19	0.09	0.2043	0.5462	0.3727	-0.1961	-0.3349	0.0164
108-662A-14H-1, 29	0.19	0.1793	0.3778	0.3781	-0.1317	-0.4699	0.0212
108-662A-14H-1, 41	0.31	0.6182	0.3557	0.2757	-0.995	-0.3217	0.0297
108-662A-14H-1, 50	0.40	0.7918	0.1492	0.2357	0.0011	-0.1388	0.0282
108-662A-14H-1, 59	0.49	0.7834	0.0748	0.3140	0.0052	-0.0565	0.0235
108-662A-14H-1, 71	0.61	0.5684	0.3594	0.4266	0.0875	-0.1379	0.0343
108-662A-14H-1, 79	0.69	0.3008	0.3049	0.4847	-0.0560	-0.1866	0.0145
108-662A-14H-1, 89	0.79	0.1577	0.1468	0.1474	-0.2995	-0.5612	0.0065
108-662A-14H-1, 101	0.91	0.1026	0.1727	0.1431	-0.2953	-0.5483	0.0055
108-662A-14H-1, 110	1.00	0.2443	0.2605	0.3667	-0.0987	-0.4519	0.0207
108-662A-14H-1, 110	1.00	0.3060	0.2228	0.3850	-0.0725	-0.5398	0.0085
108-662A-14H-1, 119	1.09	0.2342	0.2850	0.2124	-0.2468	-0.5805	0.0168
108-662A-14H-1, 131	1.21	0.0705	0.2140	0.2183	-0.2983	-0.5907	0.0076
108-662A-14H-1, 139	1.29	0.4485	0.3473	0.1628	-0.1622	-0.5370	0.0294
108-662A-14H-1, 146	1.36	0.4977	0.2924	0.2408	-0.1355	-0.4692	0.0277
108-662A-14H-2, 11	1.51	0.8719	0.1090	0.0170	0.0002	-0.1538	0.0302
108-662A-14H-2, 19	1.59	0.8578	0.2715	0.0656	-0.0005	-0.1033	0.0325
108-662A-14H-2, 29	1.69	0.6625	0.3548	0.2183	-0.0992	-0.2773	0.0287
108-662A-14H-2, 29	1.69	0.6890	0.3496	0.2569	-0.0684	-0.3231	0.0213
108-662A-14H-2, 41	1.81	0.4149	0.2996	0.1605	-0.1977	-0.5070	0.0226
108-662A-14H-2, 50	1.90	0.0817	0.2477	0.0623	-0.4057	-0.5484	0.0000
108-662A-14H-2, 59	1.99	0.2759	0.3832	0.0892	-0.2717	-0.5145	0.0169
108-662A-14H-2, 71	2.11	0.1994	0.3077	0.2190	-0.2890	-0.0521	0.0103
108-662A-14H-2, 79	2.19	0.4576	0.3032	0.2004	-0.1497	-0.4996	0.0271
108-662A-14H-2, 89	2.29	0.7364	0.2636	0.1703	-0.0711	-0.2597	0.0292
108-662A-14H-2, 101	2.41	0.8773	0.1765	0.0602	-0.0534	-0.1220	0.0275
108-662A-14H-2, 110	2.50	0.9146	0.1032	0.0131	0.0002	-0.0838	0.0293
108-662A-14H-2, 119	2.59	0.8762	0.1945	0.0062	-0.0339	-0.1721	0.0323
108-662A-14H-2, 131	2.71	0.7225	0.5535	0.0580	-0.0145	-0.1163	0.0369
108-662A-14H-2, 131	2.71	0.7417	0.5027	0.1236	0.0008	-0.1978	0.0268
108-662A-14H-2, 139	2.79	0.7018	0.4867	0.1276	0.0340	-0.2191	0.0417
108-662A-14H-2, 146	2.86	0.8127	0.3436	0.1209	0.0019	-0.1487	0.0357
108-662A-14H-2, 146	2.86	0.8400	0.3315	0.1592	0.0294	-0.2157	0.0282
108-662A-14H-3, 11	3.01	0.7469	0.4164	0.1577	0.0087	-0.1879	0.0377
108-662A-14H-3, 19	3.09	0.7970	0.3299	0.1519	0.0014	-0.2358	0.0383
108-662A-14H-3, 29	3.19	0.8138	0.3722	0.0819	-0.0262	-0.0954	0.0316
108-662A-14H-3, 41	3.31	0.8720	0.2000	-0.0116	-0.0455	-0.1318	0.0288
108-662A-14H-3, 50	3.40	0.9136	0.1395	0.0403	-0.0075	-0.0447	0.0280
108-662A-14H-3, 59	3.49	0.8972	0.1545	0.0106	0.0623	-0.0976	0.0352
108-662A-14H-3, 71	3.61	0.8853	0.2438	0.0066	-0.0561	-0.0757	0.0276
108-662A-14H-3, 79	3.69	0.7412	0.2611	0.1493	-0.0203	-0.2805	0.0341
108-662A-14H-3, 89	3.79	0.4728	0.2221	0.3012	0.0116	-0.4276	0.0332
108-662A-14H-3, 89	3.79	0.5014	0.2088	0.3304	0.0139	-0.4701	0.0393
108-662A-14H-3, 101	3.91	0.1574	0.7126	0.3616	-0.0741	-0.2424	0.0249
108-662A-14H-3, 110	4.00	0.4064	0.5841	0.3576	0.1118	-0.1863	0.0390
108-662A-14H-3, 119	4.09	0.3251	0.6962	0.3014	0.0337	-0.2447	0.0372
108-662A-14H-3, 131	4.21	0.1902	0.5587	0.3964	-0.0860	-0.3163	0.0228
108-662A-14H-3, 139	4.29	0.3744	0.4133	0.4337	0.1233	-0.2689	0.0370
108-662A-14H-3, 139	4.29	0.4209	0.3817	0.4344	0.1439	-0.3607	0.0243
108-662A-14H-3, 146	4.36	0.3326	0.2126	0.4267	-0.0899	-0.3075	0.0155
108-662A-14H-4, 11	4.51	0.1610	0.3382	0.4722	-0.0640	-0.3142	0.0165
108-662A-14H-4, 19	4.59	0.1800	0.5707	0.4515	-0.0337	-0.2182	0.0225
108-662A-14H-4, 29	4.69	0.5447	0.0676	0.4053	0.2318	-0.3166	0.0436
108-662A-14H-4, 41	4.81	0.3418	0.1360	0.5249	0.1682	-0.1427	0.0260
108-662A-14H-4, 50	4.90	0.1975	0.4622	0.5229	0.0593	-0.1348	0.0229
108-662A-14H-4, 59	4.99	0.3622	0.3724	0.4881	0.1317	-0.1546	0.0313
108-662A-14H-4, 71	5.11	0.5778	0.1210	0.3605	0.1694	-0.3899	0.0451
108-662A-14H-4, 79	5.19	0.7231	0.0553	0.2792	0.2384	-0.2777	0.0485
108-662A-14H-4, 89	5.29	0.8486	0.0571	0.1613	0.1514	-0.1988	0.0431
108-662A-14H-4, 101	5.41	0.8113	0.0724	0.1977	0.1657	-0.1788	0.0411
108-662A-14H-4, 101	5.41	0.8255	0.0695	0.2458	0.1809	-0.2260	0.0338
108-662A-14H-4, 110	5.50	0.7086	0.2117	0.2214	0.2132	-0.3052	0.0508
108-662A-14H-4, 119	5.59	0.3739	0.1915	0.2392	0.0167	-0.5811	0.0380
108-662A-14H-4, 131	5.71	0.5104	0.1559	0.3527	0.0281	-0.4490	0.0363
108-662A-14H-4, 139	5.79	0.7828	0.0945	0.1213	0.1171	-0.3156	0.0431
108-662A-14H-4, 146	5.86	0.8550	0.0646	0.1423	0.1713	-0.1311	0.0410
108-662A-14H-4, 146	5.86	0.8798	0.0507	0.1859	0.1732	-0.1936	0.0343
108-662A-14H-5, 11	6.01	0.8483	0.0696	0.0298	0.1152	-0.2626	0.0426
108-662A-14H-5, 19	6.09	0.7617	0.0586	0.0423	0.2860	-0.3596	0.0569
108-662A-14H-5, 29	6.19	0.5494	0.3316	0.2057	0.2704	-0.4783	0.0631
108-662A-14H-5, 41	6.31	0.6838	0.1205	0.2221	0.2934	-0.3263	0.0543
108-662A-14H-5, 50	6.40	0.5250	0.1308	0.3110	0.2332	-0.4338	0.0493
108-662A-14H-5, 59	6.49	0.5511	0.0884	0.3504	0.3151	-0.3400	0.0514
108-662A-14H-5, 59	6.49	0.5613	0.0438	0.4859	0.2619	-0.4302	0.0253

Table 7 (continued).

Core, section, interval (cm)	Composite depth (m)	Tropical/ subtropical	Transitional	Divergence	Upwelling	Subpolar	Polar
108-662A-14H-5, 71	6.61	0.8865	0.0351	0.1351	0.1381	-0.1022	0.0384
108-662A-14H-5, 79	6.69	0.4486	0.1079	0.2681	0.4714	-0.4529	0.0663
108-662A-14H-5, 89	6.79	0.3640	0.1781	0.1985	0.4876	-0.5488	0.0718
108-662A-14H-5, 101	6.91	0.7257	0.1744	0.0959	0.2888	-0.3704	0.0600
108-662A-14H-5, 110	7.00	0.7112	0.1783	0.1622	0.0315	-0.4054	0.0410
108-662A-14H-5, 119	7.09	0.7960	0.1435	0.1289	0.0171	-0.3263	0.0392
108-662A-14H-5, 131	7.21	0.8520	0.1605	0.1571	0.1408	-0.1613	0.0438
108-662A-14H-5, 139	7.29	0.9085	0.0535	0.0957	0.0884	-0.0888	0.0354
108-662A-14H-5, 146	7.36	0.9350	0.0374	0.0122	0.0551	-0.0260	0.0304
108-662A-14H-6, 11	7.51	0.8764	0.0396	0.1665	0.0663	-0.0251	0.0284
108-662A-14H-6, 19	7.59	0.8906	0.0421	0.1195	0.0626	-0.0383	0.0291
108-662A-14H-6, 19	7.59	0.9051	0.0222	0.2303	0.0667	-0.1273	0.0193
108-662A-14H-6, 29	7.69	0.9309	0.0357	0.0104	0.0425	-0.0210	0.0286
108-662A-14H-6, 41	7.81	0.9291	0.0338	0.0732	0.0063	-0.0090	0.0258
108-662A-14H-6, 50	7.90	0.9218	0.0327	0.0733	0.0487	-0.0012	0.0279
108-662A-14H-6, 59	7.99	0.8205	0.0616	0.1976	0.0860	-0.0708	0.0296
108-662A-14H-6, 71	8.11	0.5901	0.1266	0.3371	0.2565	-0.3519	0.0500
108-662A-14H-6, 71	8.11	0.5899	0.1015	0.5191	0.2208	-0.3590	0.0611
108-662A-14H-6, 79	8.19	0.4739	0.0916	0.4897	0.0843	-0.0529	0.0186
108-662A-14H-6, 89	8.29	0.4711	0.1383	0.4681	0.0887	-0.2740	0.0306
108-662A-14H-6, 101	8.41	0.6264	0.0694	0.3952	0.0374	-0.1561	0.0240
108-662A-14H-6, 101	8.41	0.6241	0.0605	0.5787	0.0398	-0.1737	0.0194
108-662A-14H-6, 110	8.50	0.6570	0.0606	0.3699	0.0574	-0.0809	0.0225
108-662A-14H-6, 119	8.59	0.1106	0.0703	0.5856	0.0960	-0.2151	0.0157
108-662A-14H-6, 131	8.71	0.4894	0.0704	0.4661	0.0113	-0.1262	0.0162
108-662A-14H-6, 139	8.79	0.6831	0.0536	0.3743	0.1076	-0.1003	0.0284
108-662A-14H-6, 146	8.86	0.6145	0.0662	0.3875	0.1883	-0.2674	0.0404
108-662A-14H-7, 11	9.01	0.3972	0.0577	0.3597	0.4433	-0.4629	0.0624
108-662A-14H-7, 14	9.04	0.7085	0.0544	0.1818	0.3371	-0.3130	0.0563
108-662B-6H-3, 82	9.07	0.6721	0.0575	0.3038	0.2657	-0.2490	0.0465
108-662B-6H-3, 82	9.07	0.6955	0.0361	0.4531	0.2455	-0.3153	0.0347
108-662B-6H-3, 94	9.19	0.4403	0.0647	0.4519	0.2731	-0.2739	0.0409
108-662B-6H-3, 102	9.27	0.7465	0.0515	0.2802	0.1500	-0.0885	0.0324
108-662B-6H-3, 112	9.37	0.9090	0.0484	0.0778	0.0611	-0.0080	0.0286
108-662B-6H-3, 124	9.49	0.9312	0.0710	0.0036	0.0349	0.0155	0.0274
108-662B-6H-3, 132	9.57	0.9424	0.0579	0.0013	0.0181	0.0138	0.0269
108-662B-6H-3, 142	9.67	0.9220	0.0436	0.0562	0.0179	0.0057	0.0253
108-662B-6H-4, 2	9.77	0.8883	0.0491	0.1271	0.0379	-0.0014	0.0256
108-662B-6H-4, 12	9.87	0.7829	0.0433	0.2675	0.1999	-0.1512	0.0413
108-662B-6H-4, 22	9.97	0.8055	0.0470	0.1653	0.2378	-0.1768	0.0454
108-662B-6H-4, 34	10.09	0.8667	0.0811	0.0776	0.1791	-0.1195	0.0418
108-662B-6H-4, 34	10.09	0.8800	0.0681	0.1507	0.1764	-0.2022	0.0311
108-662B-6H-4, 42	10.17	0.8862	0.0800	0.0610	0.1616	-0.1061	0.0407
108-662B-6H-4, 52	10.27	0.8808	0.1362	0.1098	0.1485	-0.1037	0.0418
108-662B-6H-4, 62	10.37	0.8888	0.0999	0.1146	0.0965	-0.0443	0.0336
108-662B-6H-4, 73	10.48	0.8644	0.0668	0.1175	0.1191	-0.0575	0.0334
108-662B-6H-4, 82	10.57	0.7802	0.0496	0.2501	0.1218	-0.0609	0.0301
108-662B-6H-4, 93	10.68	0.8811	0.0534	0.1217	0.0656	-0.0370	0.0289
108-662B-6H-4, 102	10.77	0.8864	0.0541	0.1266	0.0449	-0.0040	0.0262
108-662B-6H-4, 102	10.77	0.9038	0.0384	0.1498	0.0472	-0.0785	0.0187
108-662B-6H-4, 112	10.87	0.4719	0.2157	0.3928	-0.0581	-0.2693	0.0206
108-662B-6H-4, 124	10.99	0.4855	0.1320	0.4284	-0.0044	-0.1708	0.0180
108-662A-15H-2, 11	10.99	0.7274	0.1249	0.1901	-0.1789	-0.2182	0.0155
108-662A-15H-2, 19	11.07	0.6920	0.1680	0.3102	-0.0030	-0.0783	0.0215
108-662A-15H-2, 29	11.17	0.7452	0.1139	0.3028	-0.0364	-0.1960	0.0269
108-662A-15H-2, 41	11.29	0.7719	0.0790	0.2603	0.0301	-0.1716	0.0293
108-662A-15H-2, 50	11.38	0.7490	0.0520	0.3234	0.1063	-0.1123	0.0312
108-662A-15H-2, 59	11.47	0.8138	0.0533	0.2470	0.0386	-0.0669	0.0261
108-662A-15H-2, 71	11.59	0.9003	0.0450	0.1268	-0.0078	-0.0503	0.0254
108-662A-15H-2, 79	11.67	0.8538	0.0584	0.1026	0.1195	-0.1961	0.0394
108-662A-15H-2, 89	11.77	0.3631	0.1019	0.5279	0.0699	-0.3274	0.0285
108-662A-15H-2, 101	11.89	0.7250	0.1879	0.2746	0.1235	-0.3042	0.0457
108-662A-15H-2, 101	11.89	0.6089	0.0896	0.3909	0.0959	-0.3897	0.0099
108-662A-15H-2, 110	11.98	0.7816	0.0661	0.2502	0.0957	-0.1675	0.0341
108-662A-15H-2, 119	12.07	0.8818	0.0652	0.1413	0.0090	-0.0826	0.0277
108-662A-15H-2, 131	12.19	0.7089	0.0642	0.3460	0.0360	-0.1662	0.0275
108-662A-15H-2, 139	12.27	0.7111	0.0821	0.2570	0.0031	-0.2766	0.0301
108-662A-15H-2, 146	12.34	0.8644	0.0575	0.1168	0.0429	-0.1165	0.0301
108-662A-15H-3, 11	12.49	0.8148	0.0603	0.2302	-0.0509	-0.0914	0.0210
108-662A-15H-3, 19	12.57	0.7677	0.0882	0.2657	0.0564	-0.1203	0.0287
108-662A-15H-3, 19	12.57	0.7854	0.0579	0.2759	0.0579	-0.2384	0.0159
108-662A-15H-3, 29	12.67	0.6407	0.0989	0.3140	0.2466	-0.3834	0.0538
108-662A-15H-3, 41	12.79	0.6852	0.3534	0.2914	0.0301	-0.2056	0.0363
108-662A-15H-3, 41	12.79	0.6962	0.2703	0.2707	0.0390	-0.3581	0.0164
108-662A-15H-3, 50	12.88	0.4831	0.2120	0.4354	0.1382	-0.3565	0.0408
108-662A-15H-3, 59	12.97	0.2181	0.1176	0.3030	-0.1299	-0.5294	0.0182

Table 7 (continued).

Core, section, interval (cm)	Composite depth (m)	Tropical/subtropical	Transitional	Divergence	Upwelling	Subpolar	Polar
108-662A-15H-3, 71	13.09	0.3827	0.1105	0.2823	-0.0014	-0.5667	0.0345
108-662A-15H-3, 79	13.17	0.5322	0.1074	0.0412	0.1487	-0.6246	0.0536
108-662A-15H-3, 89	13.27	0.8573	0.0614	0.1451	-0.0423	-0.1481	0.0260
108-662A-15H-3, 101	13.39	0.9076	0.0448	0.0944	0.0219	0.0209	0.0242
108-662A-15H-3, 110	13.48	0.9108	0.0398	0.1181	0.0214	0.0167	0.0249
108-662A-15H-3, 119	13.57	0.9224	0.0341	0.0875	-0.0002	0.0146	0.0237
108-662A-15H-3, 119	13.57	0.9389	0.0177	0.1373	0.0007	-0.0622	0.0164
108-662A-15H-3, 131	13.69	0.9031	0.0637	0.1059	0.0053	0.0102	0.0238
108-662A-15H-3, 139	13.77	0.9142	0.0366	0.0862	0.0121	0.0158	0.0239
108-662A-15H-3, 146	13.84	0.8641	0.0882	0.1553	0.0527	-0.0392	0.0284
108-662A-15H-4, 11	13.99	0.7825	0.2210	0.1743	0.0452	-0.2450	0.0381
108-662A-15H-4, 19	14.07	0.0493	0.2234	0.2033	-0.3525	-0.4982	-0.0012
108-662A-15H-4, 29	14.17	0.1449	0.2375	0.1301	-0.3147	-0.5665	0.0083
108-662A-15H-4, 41	14.29	0.2567	0.4689	0.2553	-0.1497	-0.4976	0.0261
108-662A-15H-4, 41	14.29	0.2947	0.4517	0.2564	-0.1395	-0.5552	0.0194
108-662A-15H-4, 50	14.38	0.3322	0.4822	0.2433	0.3800	-0.4515	0.0680
108-662A-15H-4, 59	14.47	0.4926	0.6260	0.2165	0.0584	-0.3163	0.0462
108-662A-15H-4, 71	14.59	0.5594	0.5469	0.3281	0.0588	-0.1664	0.0392
108-662A-15H-4, 79	14.67	0.5682	0.3107	0.1482	-0.2221	-0.4094	0.0216
108-662A-15H-4, 89	14.77	0.5618	0.1271	0.3163	0.2077	-0.4728	0.0519
108-662A-15H-4, 101	14.89	0.7801	0.0851	0.2382	0.1583	-0.2370	0.0431
108-662A-15H-4, 101	14.89	0.8059	0.0709	0.2815	0.1517	-0.2934	0.0349
108-662A-15H-4, 110	14.98	0.5898	0.0488	0.0821	0.4710	-0.4405	0.0693
108-662A-15H-4, 119	15.07	0.6997	0.1082	0.2320	0.0736	-0.3609	0.0399
108-662A-15H-4, 131	15.19	0.7734	0.0876	0.0913	0.2044	-0.3077	0.0484
108-662A-15H-4, 139	15.27	0.6199	0.0816	0.1864	0.3761	-0.4369	0.0635
108-662A-15H-4, 146	15.34	0.7143	0.1352	0.2653	0.1506	-0.3216	0.0453
108-662A-15H-5, 11	15.49	0.7886	0.0986	0.1140	0.2262	-0.2939	0.0510
108-662A-15H-5, 19	15.57	0.8959	0.0451	0.0563	0.1190	-0.1171	0.0374
108-662A-15H-5, 29	15.67	0.6100	0.0670	0.3317	0.2642	-0.3723	0.0512
108-662A-15H-5, 29	15.67	0.6447	0.0349	0.3650	0.2445	-0.4720	0.0351
108-662A-15H-5, 41	15.79	0.7858	0.0507	0.2793	0.1283	-0.1790	0.0378
108-662A-15H-5, 50	15.88	0.9121	0.0359	0.0942	0.0600	-0.0252	0.0294
108-662A-15H-5, 59	15.97	0.9143	0.0434	0.0656	0.0202	-0.0351	0.0269
108-662A-15H-5, 71	16.09	0.8029	0.0558	0.2300	0.0571	-0.0772	0.0270
108-662A-15H-5, 79	16.17	0.8562	0.0536	0.1602	0.0312	-0.0653	0.0266
108-662A-15H-5, 89	16.27	0.8908	0.0425	0.1201	0.0303	-0.0120	0.0254
108-662A-15H-5, 89	16.27	0.9060	0.0225	0.1814	0.0410	-0.1176	0.0141
108-662A-15H-5, 101	16.39	0.9143	0.0375	0.0979	0.0656	-0.0730	0.0328
108-662A-15H-5, 110	16.48	0.8205	0.0390	0.1670	0.2379	-0.2244	0.0497
108-662A-15H-5, 119	16.57	0.8771	0.0522	0.0753	0.1680	-0.1861	0.0446
108-662A-15H-5, 131	16.69	0.8104	0.1163	0.2126	0.1324	-0.2351	0.0461
108-662A-15H-5, 139	16.77	0.4969	0.3390	0.2547	0.3239	-0.4685	0.0659
108-662A-15H-5, 146	16.84	0.4959	0.4614	0.2673	0.2457	-0.4078	0.0601
108-662A-15H-6, 11	16.99	0.4217	0.1322	0.3731	0.2803	-0.4409	0.0502
108-662A-15H-6, 11	16.99	0.4473	0.1143	0.4330	0.2689	-0.4638	0.0430
108-662A-15H-6, 19	17.07	0.7040	0.0817	0.3066	0.1438	-0.2298	0.0381
108-662A-15H-6, 29	17.17	0.8333	0.0425	0.2381	0.1185	-0.1368	0.0369
108-662A-15H-6, 41	17.29	0.6168	0.1770	0.1469	-0.0893	-0.4402	0.0308
108-662A-15H-6, 50	17.38	0.6559	0.0824	0.1996	0.2042	-0.4188	0.0496
108-662A-15H-6, 59	17.47	0.4141	0.1078	0.3576	-0.0501	-0.4246	0.0241
108-662A-15H-6, 71	17.59	0.5348	0.0682	0.4132	0.2251	-0.3037	0.0421
108-662A-15H-6, 79	17.67	0.8373	0.0466	0.2188	0.1009	-0.1017	0.0333
108-662A-15H-6, 89	17.77	0.9081	0.0383	0.0670	0.0423	0.0051	0.0260
108-662A-15H-6, 101	17.89	0.8856	0.0353	0.1684	0.0239	0.0216	0.0236
108-662A-15H-6, 110	17.98	0.7872	0.0555	0.2289	0.1704	-0.2003	0.0412
108-662A-15H-6, 119	18.07	0.7878	0.0653	0.1644	0.2460	-0.2384	0.0489
108-662A-15H-6, 131	18.19	0.7054	0.0601	0.2696	0.2447	-0.2853	0.0481
108-662A-15H-6, 131	18.19	0.7216	0.0409	0.3421	0.2326	-0.3485	0.0360
108-662A-15H-6, 139	18.27	0.5290	0.0582	0.3384	0.3457	-0.4457	0.0591
108-662A-15H-6, 146	18.34	0.7179	0.0748	0.1919	0.1825	-0.3653	0.0477
108-662A-15H-7, 11	18.49	0.6605	0.0707	0.1919	0.2978	-0.4085	0.0565
108-662A-15H-7, 19	18.57	0.8254	0.0724	0.1441	0.0307	-0.2084	0.0324
108-662A-15H-7, 29	18.67	0.8722	0.0463	0.1233	0.0542	-0.0206	0.0265
108-662A-15H-7, 41	18.79	0.9179	0.0392	0.0471	0.0082	0.0076	0.0239

Note: Full assemblage counts (second value listed) and quick counts with seven species (first value listed) are given; spliced record. Factor loadings can vary between +1.0 and -1.0.

Pliocene and late Pleistocene. This provides additional evidence that the orbital-band responses of these two regions are largely independent.

Thus, the SST response of the equatorial Atlantic divergence region must largely reflect an interaction with parts of the climate system other than the middle to high latitudes of

the Northern Hemisphere. Two possibilities are likely: (1) influence from the Southern Hemisphere (subantarctic) on Benguela Current flow and on trade-wind-modulated divergence (Gardner and Hays, 1976; Mix et al., 1986a, 1986b; McIntyre et al., 1989), and (2) interactions with the African monsoon (Mix et al., 1986a, 1986b; McIntyre et al., 1989).

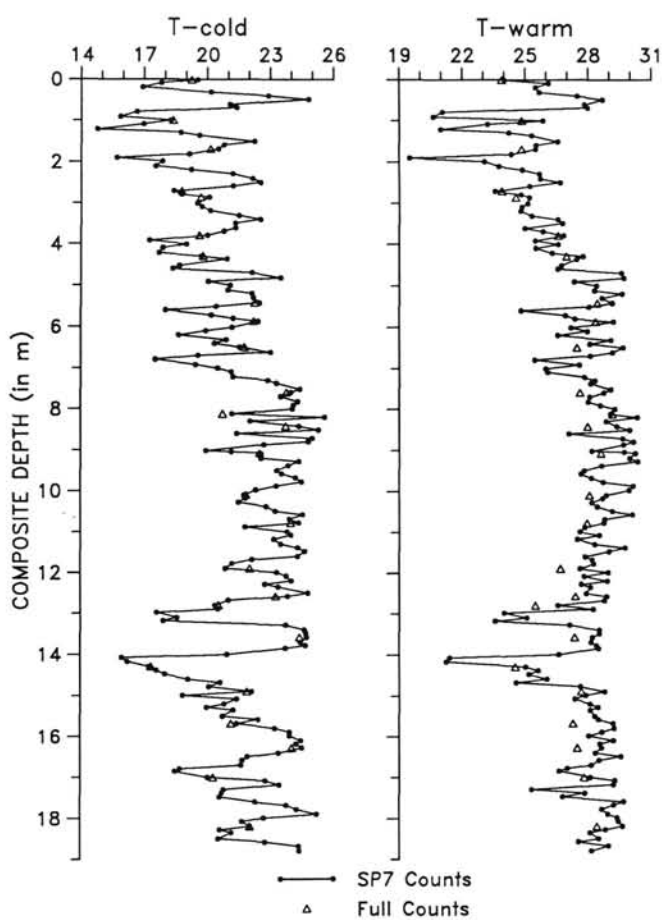


Figure 11. Variations in estimated sea-surface temperature (in °C), Site 662 (spliced) for cold-season (T-cold) and warm-season (T-warm), including quick counts with seven species (SP7) and intermittent full assemblage counts.

In their study of the eastern equatorial Atlantic of the last 3.5 m.y., Ruddiman and Janecek (this vol.) note an increased flux of opal and terrigenous dust roughly coincident with the initiation of moderate-scale Northern Hemisphere glaciation near 2.4 Ma. Although this finding might be interpreted as evidence that equatorial and Northern Hemisphere circulation are, in fact, interdependent, Ruddiman and Janecek argue that the more immediate control of the equatorial ocean is the subantarctic ocean, as suggested from late Pleistocene orbital variations (McIntyre et al., 1989). Subsequent high-resolution studies of cores from the Southern Hemisphere and the equatorial Atlantic are needed to clarify the possible connections between these regions over the last few million years.

ACKNOWLEDGMENTS

We thank Linda Baker and Pat Malone for preparation of Site 662 samples; Ann Esmay for assembling the tables and figures; Christina Hardy for oxygen isotope analyses; Barbara Molfino for advice on signal interpretation; Maureen Raymo for assistance with the tuned isotopic time scale; Beatrice Rasmussen for help in assembling the manuscript; and Kathy Tedesco for preparation and faunal analyses of some RC24-7 samples. We also thank James D. Hays and George Kukla for internal reviews, and Alan C. Mix and Uwe Pfleidermann for constructive criticisms. This work was supported by the Ocean Sciences Program of the National Science Foundation (Grants OCE86-08328 and OCE85-16133). This is Lamont-Doherty Geological Observatory Contribution No. 4402.

Table 8. Site 662 estimated sea-surface temperatures.

Core, section, interval (cm)	Composite depth (m)	T-warm	T-cold
108-662A-14H-1, 11	0.01	24.02	19.53
108-662A-14H-1, 11	0.01	23.89	19.25
108-662A-14H-1, 19	0.09	26.12	17.81
108-662A-14H-1, 29	0.19	25.50	16.93
108-662A-14H-1, 41	0.31	25.69	20.17
108-662A-14H-1, 50	0.40	27.49	22.91
108-662A-14H-1, 59	0.49	28.68	24.82
108-662A-14H-1, 71	0.61	27.83	21.06
108-662A-14H-1, 79	0.69	27.97	21.39
108-662A-14H-1, 89	0.79	21.06	16.64
108-662A-14H-1, 101	0.91	20.62	15.86
108-662A-14H-1, 110	1.00	25.85	18.26
108-662A-14H-1, 110	1.00	24.83	18.36
108-662A-14H-1, 119	1.09	23.21	16.97
108-662A-14H-1, 131	1.21	20.97	14.77
108-662A-14H-1, 139	1.29	24.21	18.72
108-662A-14H-1, 146	1.36	25.30	19.61
108-662A-14H-2, 11	1.51	26.55	22.24
108-662A-14H-2, 19	1.59	25.53	20.79
108-662A-14H-2, 29	1.69	25.50	20.52
108-662A-14H-2, 29	1.69	24.83	20.15
108-662A-14H-2, 41	1.81	24.34	19.15
108-662A-14H-2, 50	1.90	19.50	15.71
108-662A-14H-2, 59	1.99	23.07	17.87
108-662A-14H-2, 71	2.11	23.76	17.54
108-662A-14H-2, 79	2.19	24.86	19.24
108-662A-14H-2, 89	2.29	25.68	21.20
108-662A-14H-2, 101	2.41	25.73	22.15
108-662A-14H-2, 110	2.50	26.66	22.52
108-662A-14H-2, 119	2.59	25.21	21.22
108-662A-14H-2, 131	2.71	23.56	18.40
108-662A-14H-2, 131	2.71	23.88	18.78
108-662A-14H-2, 139	2.79	24.80	18.77
108-662A-14H-2, 146	2.86	25.19	20.07
108-662A-14H-2, 146	2.86	24.55	19.68
108-662A-14H-3, 11	3.01	25.12	19.52
108-662A-14H-3, 19	3.09	24.83	19.73
108-662A-14H-3, 29	3.19	24.78	20.12
108-662A-14H-3, 41	3.31	25.30	21.49
108-662A-14H-3, 50	3.40	26.55	22.51
108-662A-14H-3, 59	3.49	26.76	21.31
108-662A-14H-3, 71	3.61	24.99	21.34
108-662A-14H-3, 79	3.69	25.85	20.78
108-662A-14H-3, 89	3.79	26.82	20.00
108-662A-14H-3, 89	3.79	26.57	19.62
108-662A-14H-3, 101	3.91	25.48	17.26
108-662A-14H-3, 110	4.00	26.57	19.00
108-662A-14H-3, 119	4.09	25.50	17.88
108-662A-14H-3, 131	4.21	26.28	17.70
108-662A-14H-3, 139	4.29	27.75	19.70
108-662A-14H-3, 139	4.29	26.96	19.79
108-662A-14H-3, 146	4.36	27.44	20.93
108-662A-14H-4, 11	4.51	26.71	18.67
108-662A-14H-4, 19	4.59	26.54	18.36
108-662A-14H-4, 29	4.69	29.57	22.12
108-662A-14H-4, 41	4.81	29.67	23.48
108-662A-14H-4, 50	4.90	27.32	20.02
108-662A-14H-4, 59	4.99	28.38	21.07
108-662A-14H-4, 71	5.11	28.27	20.96
108-662A-14H-4, 79	5.19	29.58	22.11
108-662A-14H-4, 89	5.29	28.63	22.17
108-662A-14H-4, 101	5.41	29.12	22.46
108-662A-14H-4, 101	5.41	28.41	22.25
108-662A-14H-4, 110	5.50	28.02	20.41
108-662A-14H-4, 119	5.59	24.80	18.02
108-662A-14H-4, 131	5.71	26.91	20.18
108-662A-14H-4, 139	5.79	27.36	21.23
108-662A-14H-4, 146	5.86	29.19	22.42
108-662A-14H-4, 146	5.86	28.34	22.21
108-662A-14H-5, 11	6.01	27.18	21.17
108-662A-14H-5, 19	6.09	27.95	19.92
108-662A-14H-5, 29	6.19	26.54	18.63
108-662A-14H-5, 41	6.31	29.07	20.89
108-662A-14H-5, 50	6.40	28.06	20.33
108-662A-14H-5, 59	6.49	29.64	21.54
108-662A-14H-5, 59	6.49	27.45	21.75

Table 8 (continued).

Core, section, interval (cm)	Composite depth (m)	T-warm	T-cold
108-662A-14H-5, 71	6.61	29.13	22.99
108-662A-14H-5, 79	6.69	28.08	19.55
108-662A-14H-5, 89	6.79	25.44	17.52
108-662A-14H-5, 101	6.91	27.56	19.43
108-662A-14H-5, 110	7.00	25.96	20.49
108-662A-14H-5, 119	7.09	26.05	21.13
108-662A-14H-5, 131	7.21	27.80	21.21
108-662A-14H-5, 139	7.29	28.30	22.87
108-662A-14H-5, 146	7.36	28.09	23.27
108-662A-14H-6, 11	7.51	29.07	24.40
108-662A-14H-6, 19	7.59	28.74	23.97
108-662A-14H-6, 19	7.59	27.60	23.76
108-662A-14H-6, 29	7.69	28.05	23.49
108-662A-14H-6, 41	7.81	27.99	24.30
108-662A-14H-6, 50	7.90	28.56	24.09
108-662A-14H-6, 59	7.99	29.26	24.04
108-662A-14H-6, 71	8.11	29.04	21.17
108-662A-14H-6, 71	8.11	29.12	20.73
108-662A-14H-6, 79	8.19	30.31	25.57
108-662A-14H-6, 89	8.29	28.83	22.03
108-662A-14H-6, 101	8.41	29.34	24.34
108-662A-14H-6, 101	8.41	27.96	23.72
108-662A-14H-6, 110	8.50	29.95	25.27
108-662A-14H-6, 119	8.59	27.06	21.39
108-662A-14H-6, 131	8.71	29.61	24.97
108-662A-14H-6, 139	8.79	30.12	24.78
108-662A-14H-6, 146	8.86	29.65	22.68
108-662A-14H-7, 11	9.01	28.14	19.92
108-662A-14H-7, 14	9.04	29.68	21.13
108-662B-6H-3, 82	9.07	30.20	22.53
108-662B-6H-3, 82	9.07	28.58	22.48
108-662B-6H-3, 94	9.19	29.93	22.53
108-662B-6H-3, 102	9.27	30.31	24.33
108-662B-6H-3, 112	9.37	28.60	23.82
108-662B-6H-3, 124	9.49	27.79	23.30
108-662B-6H-3, 132	9.57	27.65	23.53
108-662B-6H-3, 142	9.67	28.13	24.19
108-662B-6H-4, 2	9.77	28.70	24.48
108-662B-6H-4, 12	9.87	30.11	23.27
108-662B-6H-4, 22	9.97	29.92	22.30
108-662B-6H-4, 34	10.09	28.84	21.74
108-662B-6H-4, 34	10.09	28.04	21.84
108-662B-6H-4, 42	10.17	28.66	21.82
108-662B-6H-4, 52	10.27	28.15	21.48
108-662B-6H-4, 62	10.37	28.40	22.79
108-662B-6H-4, 73	10.48	29.12	23.22
108-662B-6H-4, 82	10.57	30.07	24.52
108-662B-6H-4, 93	10.68	28.75	23.89
108-662B-6H-4, 102	10.77	28.71	24.33
108-662B-6H-4, 102	10.77	27.92	23.96
108-662B-6H-4, 112	10.87	27.82	21.80
108-662B-6H-4, 124	10.99	29.04	23.75
108-662A-15H-2, 11	10.99	26.12	23.82
108-662A-15H-2, 19	11.07	28.50	23.96
108-662A-15H-2, 29	11.17	27.45	23.15
108-662A-15H-2, 41	11.29	28.28	23.48
108-662A-15H-2, 50	11.38	29.71	24.28
108-662A-15H-2, 59	11.47	28.96	24.62
108-662A-15H-2, 71	11.59	27.83	24.29
108-662A-15H-2, 79	11.67	28.17	22.13
108-662A-15H-2, 89	11.77	28.24	21.18
108-662A-15H-2, 101	11.89	27.59	20.86
108-662A-15H-2, 101	11.89	26.67	22.03
108-662A-15H-2, 110	11.98	28.92	23.30
108-662A-15H-2, 119	12.07	27.78	23.75
108-662A-15H-2, 131	12.19	28.88	23.99
108-662A-15H-2, 139	12.27	27.65	22.73
108-662A-15H-2, 146	12.34	28.08	23.36
108-662A-15H-3, 11	12.49	27.87	24.77
108-662A-15H-3, 19	12.57	28.84	23.81
108-662A-15H-3, 19	12.57	27.36	23.24
108-662A-15H-3, 29	12.67	28.74	20.99
108-662A-15H-3, 41	12.79	26.53	20.37

Table 8 (continued).

Core, section, interval (cm)	Composite depth (m)	T-warm	T-cold
108-662A-15H-3, 41	12.79	25.46	20.52
108-662A-15H-3, 50	12.88	28.20	20.50
108-662A-15H-3, 59	12.97	23.97	17.61
108-662A-15H-3, 71	13.09	25.05	18.56
108-662A-15H-3, 79	13.17	23.55	17.91
108-662A-15H-3, 89	13.27	27.08	23.71
108-662A-15H-3, 101	13.39	28.48	24.59
108-662A-15H-3, 110	13.48	28.50	24.68
108-662A-15H-3, 119	13.57	28.17	24.72
108-662A-15H-3, 119	13.57	27.33	24.39
108-662A-15H-3, 131	13.69	28.10	24.42
108-662A-15H-3, 139	13.77	28.36	24.66
108-662A-15H-3, 146	13.84	28.45	23.71
108-662A-15H-4, 11	13.99	26.57	20.94
108-662A-15H-4, 19	14.07	21.40	15.96
108-662A-15H-4, 29	14.17	21.23	16.22
108-662A-15H-4, 41	14.29	24.99	17.25
108-662A-15H-4, 41	14.29	24.51	17.34
108-662A-15H-4, 50	14.38	25.60	17.60
108-662A-15H-4, 59	14.47	25.14	18.00
108-662A-15H-4, 71	14.59	26.01	19.08
108-662A-15H-4, 79	14.67	24.54	20.61
108-662A-15H-4, 89	14.77	27.59	20.07
108-662A-15H-4, 101	14.89	28.74	22.10
108-662A-15H-4, 101	14.89	27.64	21.88
108-662A-15H-4, 110	14.98	27.84	18.82
108-662A-15H-4, 119	15.07	27.32	21.39
108-662A-15H-4, 131	15.19	28.04	20.79
108-662A-15H-4, 139	15.27	28.42	19.96
108-662A-15H-4, 146	15.34	28.05	21.22
108-662A-15H-5, 11	15.49	28.28	20.73
108-662A-15H-5, 19	15.57	28.45	22.42
108-662A-15H-5, 29	15.67	29.15	21.40
108-662A-15H-5, 29	15.67	27.25	21.13
108-662A-15H-5, 41	15.79	29.19	23.20
108-662A-15H-5, 50	15.88	28.62	23.90
108-662A-15H-5, 59	15.97	27.99	23.90
108-662A-15H-5, 71	16.09	29.15	24.43
108-662A-15H-5, 79	16.17	28.51	24.20
108-662A-15H-5, 89	16.27	28.59	24.49
108-662A-15H-5, 89	16.27	27.45	24.00
108-662A-15H-5, 101	16.39	28.30	23.37
108-662A-15H-5, 110	16.48	29.51	21.89
108-662A-15H-5, 119	16.57	28.47	21.65
108-662A-15H-5, 131	16.69	28.10	21.59
108-662A-15H-5, 139	16.77	26.97	18.68
108-662A-15H-5, 146	16.84	26.57	18.46
108-662A-15H-6, 11	16.99	28.05	20.00
108-662A-15H-6, 11	16.99	27.76	20.26
108-662A-15H-6, 19	17.07	29.21	22.74
108-662A-15H-6, 29	17.17	29.14	23.40
108-662A-15H-6, 41	17.29	25.26	20.75
108-662A-15H-6, 50	17.38	27.79	20.66
108-662A-15H-6, 59	17.47	26.75	20.59
108-662A-15H-6, 71	17.59	29.64	22.27
108-662A-15H-6, 79	17.67	29.17	23.74
108-662A-15H-6, 89	17.77	28.60	24.23
108-662A-15H-6, 101	17.89	28.89	25.19
108-662A-15H-6, 110	17.98	29.32	22.68
108-662A-15H-6, 119	18.07	29.38	21.64
108-662A-15H-6, 131	18.19	29.58	22.03
108-662A-15H-6, 131	18.19	28.38	22.02
108-662A-15H-6, 139	18.27	28.78	20.59
108-662A-15H-6, 146	18.34	28.05	21.14
108-662A-15H-7, 11	18.49	28.46	20.51
108-662A-15H-7, 19	18.57	27.50	22.74
108-662A-15H-7, 29	18.67	28.92	24.33
108-662A-15H-7, 41	18.79	28.12	24.36

Note: Warm-season (T-warm) and cold-season (T-cold) estimates (in °C) are based on full assemblage counts (second value listed) and quick counts with seven species (SP7; first value listed).

Table 9. Statistics of Site 662 (spliced record) estimated sea-surface temperatures and %CaCO₃.

	Season	No. of samples	Minimum	Maximum	Mean	Variance	Standard deviation
Site 662	T-warm	28	23.88	29.12	26.91	2.29	1.51
(full)	T-cold	28	17.34	24.39	21.43	3.55	1.88
Site 662	T-warm	191	19.50	30.31	27.39	4.13	2.03
(SP7)	T-cold	191	14.77	25.57	21.47	5.52	2.35
%CaCO ₃	—	191	61.64	92.69	83.88	35.54	5.96

Note: Warm-season (T-warm) and cold-season (T-cold) estimates (in °C) are based on full assemblage counts (full) and quick counts with seven species (SP7).

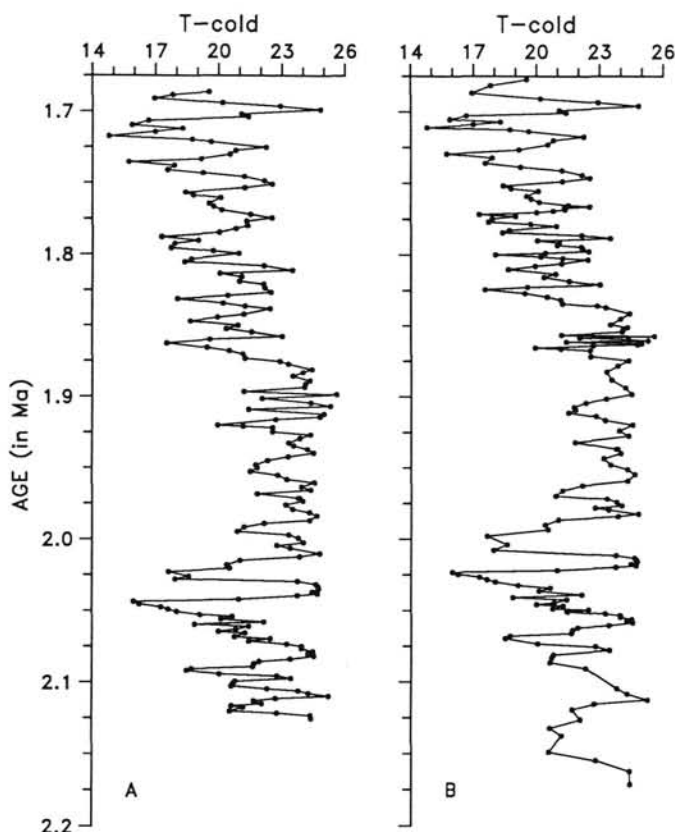


Figure 12. Variations in estimated sea-surface temperature (in °C), Site 662 (spliced); cold-season (T-cold) estimates based on quick counts with seven species. A. Biostratigraphic time scale. B. Tuned time scale.

REFERENCES

- Backman, J., 1979. Pliocene biostratigraphy of DSDP Sites 111 and 116 from the North Atlantic Ocean and the age of Northern Hemisphere glaciation. *Stockholm Contrib. Geol.*, 32:115–137.
- , 1985. Cenozoic calcareous nannofossil biostratigraphy from the northeastern Atlantic Ocean Deep Sea Drilling Project Leg 81. In Roberts, D. G., Schnitker, D., et al., *Init. Repts. DSDP*, 81: Washington (U.S. Govt. Printing Office), 403–428.
- Backman, J., and Pestiaux, P., 1986. Pliocene *Discoaster* abundance variations, Deep Sea Drilling Project Site 606: biochronology and paleoenvironmental implications. In Ruddiman, W. F., Kidd, R. B., Thomas, E., et al., *Init. Repts. DSDP*, 94, Pt. 2: Washington (U.S. Govt. Printing Office), 903–910.
- Baldauf, J. G., Thomas, E., Clement, B., Takayama, T., Weaver, P. P. E., Backman, J., and Westberg-Smith, M. J., 1986. Magnetostratigraphic and biostratigraphic synthesis, Deep Sea Drilling Project Leg 94. In Ruddiman, W. F., Kidd, R. B., Thomas, E., et al., *Init. Repts. DSDP*, 94, Pt. 2: Washington (U.S. Govt. Printing Office), 1159–1206.
- Berger, W., 1968. Planktonic foraminifera: selective solution and paleoclimatic interpretation. *Deep-Sea Res.*, 15:31–43.
- Curry, W. B., and Lohmann, G. P., 1986. Late Quaternary carbonate sedimentation at the Sierra Leone Rise (eastern equatorial Atlantic Ocean). *Mar. Geo.*, 70:223–250.
- Fairbanks, R. G., Sverdrup, M., Free, R., Wiebe, P. H., and Bé, A. W. H., 1982. Vertical distribution and isotopic fractionation of living planktonic foraminifera from the Panama Basin. *Nature*, 298:841–844.
- Gardner, J., and Hays, J. D., 1976. Responses of sea-surface temperature and circulation to global climatic change during the past 200,000 years in the eastern equatorial Atlantic Ocean. In Cline, R. M., and Hays, J. D. (Eds.), *Investigation of Late Quaternary Paleoceanography and Paleoclimatology*. Mem. Geol. Soc. Am., 145:221–246.
- Hays, J. D., Imbrie, J. I., and Shackleton, N. J., 1976. Variations in the earth's orbit: pacemaker of the ice ages. *Science*, 194:1121–1132.
- Hutson, W. H., 1977. Transfer functions under no-analog conditions: experiments with Indian Ocean planktonic foraminifera. *Quat. Res.*, 8:355–367.
- Imbrie, J., Hays, J., Martinson, D., McIntyre, A., Mix, A., Morley, J., Pisias, N., Prell, W., and Shackleton, N. J., 1984. The orbital theory of Pleistocene climate: support for a revised chronology of the marine δ¹⁸O record. In Berger, A., Imbrie, J., Hays, J., Kukla, G., and Saltzman, B. (Eds.), *Milankovitch and Climate* (Vol. 1): Hingham, MA (D. Reidel), 269–305.
- Imbrie, J., McIntyre, A., and Mix, A. C., in press. Oceanic response to orbital forcing in the late Quaternary: observational and experimental strategies. In Duplessy, J.-C., Berger, A., and

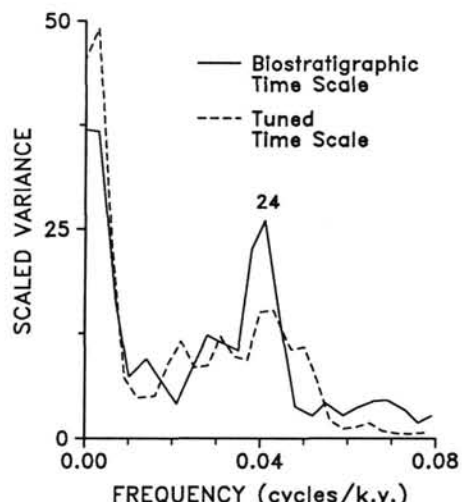


Figure 13. Variance spectra of estimated sea-surface temperature, Site 662 (spliced); cold-season (T-cold) estimates based on quick counts with seven species. Band width = 0.009 and 0.008 for the biostratigraphic and tuned time scales, respectively.

- Schneider, S. H. (Eds.), *Climate and Geosciences*: Hingham, MA (D. Reidel).
- Karlin, K., 1986. Development of a method of streamlining foraminiferal census counts for equatorial Atlantic Ocean cores [Master's research]. Columbia Univ.
- Kipp, N., 1976. New transfer function for estimating past sea-surface conditions from sea-bed distribution of planktonic foraminiferal assemblages in the North Atlantic. In Cline, R. M., and Hays, J. D. (Eds.), *Investigation of Late Quaternary Paleoceanography and Paleoclimatology*. Mem. Geol. Soc. Am., 145:3-41.
- McIntyre, A., Ruddiman, W. F., Karlin, K., and Mix, A. C., 1989. Surface water response of the equatorial Atlantic Ocean to orbital forcing. *Paleoceanography*, 4:19-55.
- Malmgren, B. A., and Kennett, J. P., 1981. Phyletic gradualism in a late Cenozoic planktonic foraminiferal lineage; DSDP Site 284, southwest Pacific. *Paleobiology*, 7:230-240.
- Martinson, D. G., Menke, W., and Stoffa, P., 1982. An inverse approach to signal correlation. *J. Geophys. Res.*, 87:4807-4818.
- Martinson, D. G., Pisias, N. G., Hays, J. D., Imbrie, J., Moore, T. C., and Shackleton, N. J., 1987. Age dating and the orbital theory of the ice ages: development of a high-resolution 0 to 300,000-year chronostratigraphy. *Quat. Res.*, 27:1-29.
- Mix, A. C., Ruddiman, W. F., and McIntyre, A., 1986a. Late Quaternary paleoceanography of the tropical Atlantic, 1: spatial variability of annual mean sea-surface temperatures, 0-20,000 years B.P. *Paleoceanography*, 1:43-66.
- , 1986b. Late Quaternary paleoceanography of the tropical Atlantic, 2: the seasonal cycle of sea surface temperatures, 0-20,000 years B.P. *Paleoceanography*, 1:339-353.
- Molfino, B., Kipp, N. G., and Morley, J. J., 1982. Comparison of foraminiferal, coccolithophorid, and radiolarian paleotemperature equations: assemblage coherency and estimate concordancy. *Quat. Res.*, 17:279-313.
- Parker, F. L., and Berger, W. H., 1971. Faunal and solution patterns of planktonic foraminifera in surface sediments of the South Pacific. *Deep-Sea Res.*, 18:73-107.
- Pisias, N. G., and Moore, T. C., 1981. The evolution of Pleistocene climate: a time series approach. *Earth Planet. Sci. Lett.*, 52:450-458.
- Prell, W. L., 1982. Oxygen and carbon isotope stratigraphy for the Quaternary of Hole 502B: evidence for two modes of isotopic variability. In Prell, W. L., Gardner, J. V., et al., *Init. Repts. DSDP*, 68: Washington (U.S. Govt. Printing Office), 455-464.
- Raymo, M. E., Ruddiman, W. F., Backman, J., Clement, B. M., and Martinson, D. G., in press. Late Pliocene variation in Northern Hemisphere ice sheets and North Atlantic Deep Water circulation. *Paleoceanography*.
- Raymo, M., Ruddiman, W. F., and Clement, B. M., 1986. Pliocene-Pleistocene paleoceanography of the North Atlantic at Deep Sea Drilling Project Site 609. In Ruddiman, W. F., Kidd, R. B., Thomas, E., et al., *Init. Repts. DSDP*, 94, Pt. 2: Washington (U.S. Govt. Printing Office), 895-901.
- Ruddiman, W. F., Backman, J., Baldauf, J., Hooper, P., Keigwin, L., Miller, K., Raymo, M., and Thomas, E., 1986a. Leg 94 paleoenvironmental synthesis. In Ruddiman, W. F., Kidd, R. B., Thomas, E., et al., *Init. Repts. DSDP*, 94, Pt. 2: Washington (U.S. Govt. Printing Office), 1207-1215.
- Ruddiman, W. F., and Esmay, A., 1986. A streamlined foraminiferal transfer function for the subpolar North Atlantic. In Ruddiman, W. F., Kidd, R. B., Thomas, E., et al., *Init. Repts. DSDP*, 94, Pt. 2: Washington (U.S. Govt. Printing Office), 1045-1060.
- Ruddiman, W. F., and Heezen, B. C., 1967. Differential solution of planktonic foraminifera. *Deep-Sea Res.*, 14:801-808.
- Ruddiman, W. F., and McIntyre, A., 1981. Oceanic mechanisms for the amplification of the 23,000-year ice-volume cycle. *Science*, 212:617-627.
- , 1984. Ice-age thermal response and climatic role of the surface Atlantic Ocean, 40°N to 63°N. *Geol. Soc. Am. Bull.*, 95:381-396.
- Ruddiman, W. F., McIntyre, A., and Raymo, M., 1986b. Paleoenvironmental results from North Atlantic Sites 607 and 609. In Ruddiman, W. F., Kidd, R. B., Thomas, E., et al., *Init. Repts. DSDP*, 94, Pt. 2: Washington (U.S. Govt. Printing Office), 855-878.
- Ruddiman, W. F., Raymo, M., and McIntyre, A., 1986c. Matuyama 41,000-year cycles: North Atlantic Ocean and northern hemisphere ice sheets. *Earth Planet. Sci. Lett.*, 80:117-129.
- Ruddiman, W. F., Shackleton, N. J., and McIntyre, A., 1986d. North Atlantic sea-surface temperatures for the last 1.1 million years. In Summerhayes, C. P., and Shackleton, N. J. (Eds.), *North Atlantic Paleoceanography*. Geol. Soc. Spec. Publ. (London), 21:155-173.
- Shackleton, N. J., Backman, J., Zimmerman, H., Kent, D. V., Hall, M. A., Roberts, D. G., Schnitker, D., Baldauf, J. G., Desprairies, A., Homrighausen, R., Huddlestun, P., Keene, J. B., Kaltenback, A. J., Krumsiek, K. A., Morton, A. C., Murray, J. W., and Westberg-Smith, J., 1984. Oxygen isotope calibration of the onset of ice-rafting and history of glaciation in the North Atlantic region. *Nature*, 307:620-623.
- Shackleton, N. J., and Opdyke, N. D., 1973. Oxygen isotope and paleomagnetic stratigraphy of equatorial Pacific core V28-238: oxygen isotope temperatures and ice volumes on a 10⁵ year and 10⁶ year scale. *Quat. Res.*, 3:39-55.
- Shipboard Scientific Party, 1988. Site 662. In Ruddiman, W. F., Sarnthein, M., et al., *Proc. ODP, Init. Repts.*, 108: College Station, TX (Ocean Drilling Program), 487-556.
- SPECMAP Archive 1, 1989. Data Support Section, National Center for Atmospheric Research, Boulder, CO.
- Takahashi, T., Broecker, W. S., Bainbridge, A. E., and Weiss, R. F., 1980. Carbonate chemistry of the Atlantic, Pacific, and Indian Oceans: the results of the GEOSECS expeditions, 1972-1978. *Lamont-Doherty Geol. Observ. Tech. Rept. No. 1*, CU-I-80.
- Thunell, R. C., and Honjo, S., 1981. Calcite dissolution and the modification of planktonic foraminiferal assemblages. *Mar. Micropaleontol.*, 6:169-182.
- Zimmerman, H. B., Shackleton, N. J., Backman, J., Kent, D. V., Baldauf, J. G., Kaltenback, A. J., and Morton, A. C., 1985. History of Plio-Pleistocene climate in the northeastern Atlantic, Deep Sea Drilling Project Hole 552A. In Roberts, D. G., Schnitker, D., et al., *Init. Repts. DSDP*, 81: Washington (U.S. Govt. Printing Office), 861-875.

Date of initial receipt: 2 May 1988

Date of acceptance: 12 February 1989

Ms 108B-164

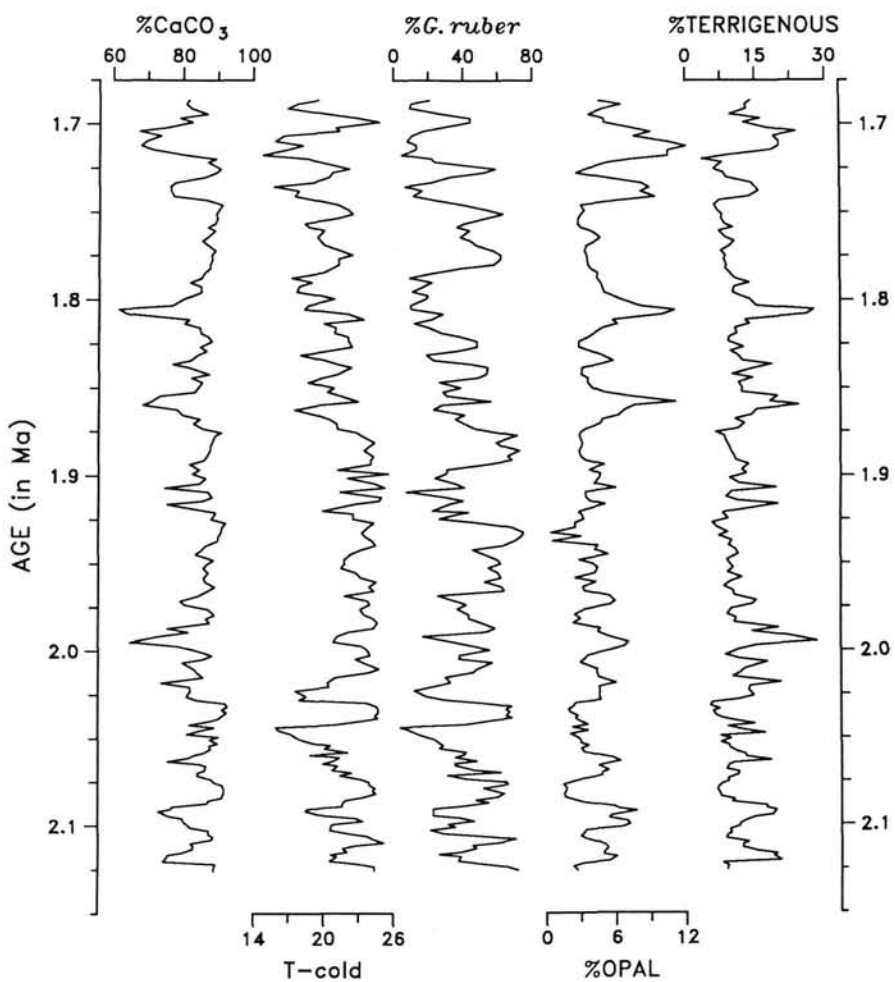


Figure 14. Variations in $\% \text{CaCO}_3$, estimated sea-surface temperature in $^{\circ}\text{C}$ (T-cold [cold-season] based on quick counts with seven species), $\% \text{Globigerinoides ruber}$ (var. white), $\% \text{opal}$, and $\% \text{terrigenous}$ component, for Site 662 (spliced), according to the biostratigraphic time scale. The choice of this time scale to represent the five parameters was arbitrary.

Table 10. Site 662 (spliced record) cross-spectral results of $\% \text{CaCO}_3$ vs. sea-surface temperature estimates and vs. $\% \text{G. ruber}$ (w).

	Season	r	Coherency ²	^a Phase (k.y.)
Biostratigraphic time scale:				
$\% \text{CaCO}_3$ vs.	T-warm	0.17	^b 0.58	^b -3.4
SST	T-cold	0.38	^b 0.80	^b -2.6
$\% \text{CaCO}_3$ vs.	—	0.55	^b 0.86	^b -2.7
$\% \text{G. ruber}$ (w)				
Tuned time scale:				
$\% \text{CaCO}_3$ vs.	T-warm	0.17	^c 0.32	^c -2.6
SST	T-cold	0.42	^d 0.75	^d -1.4
$\% \text{CaCO}_3$ vs.	—	0.53	^c 0.82	^c -2.3
$\% \text{G. ruber}$ (w)				

Note: Warm-season (T-warm) and cold-season (T-cold) estimates (in $^{\circ}\text{C}$) are based on quick counts with seven species. 95% confidence interval; bandwidth = 0.022; r = correlation coefficient; SST = sea-surface temperature.

^a Quantity listed first leads second quantity when phasing is positive; quantity listed first lags second quantity when phasing is negative.

^b At a period of 24.2 k.y.

^c At a period of 26.0 k.y.

^d At a period of 24.8 k.y.